BANDGAP ENGINEERING OF MULTIFERROIC BISMUTH FERRITE FOR PHOTOVOLTAIC APPLICATION

A THESIS IS SUBMITTED IN PARTIAL FULFILLMENT OF THE REQUIREMENTS FOR THE DEGREE OF BACHELOR OF SCIENCE IN ELECTRICAL & ELECTRONIC ENGINEERING

BY

RUSSEL MAHBUB	**15.01.05.169**
MD. GOLAM MUNTAKIM	**14.01.05.085**
SHARMIN AKTER	**13.02.05.089**



DEPARTMENT OF ELECTRICAL & ELECTRONIC ENGINEERING

AHSANULLAH UNIVERSITY OF SCIENCE & TECHNOLOGY

FALL 2018. SPRING 2019

APPROVAL

This is to certify that, the thesis entitled **"Bandgap Engineering of Multiferroic Bismuth Ferrite for PV Application"** is written by Russel Mahbub, Md. Golam Muntakim and Sharmin Akter under my direct supervision**.** They have successfully defended their thesis work.

Supervisor

.....

Md. Meganur Rhaman

Associate Professor

Department of Electrical and Electronic Engineering

Ahsanullah University of Science and Technology

DECLARATION

It is hereby declared that, except where specific references are made to other investigations, the work embodied in this thesis is the result of investigation carried out by the authors under the supervision of Md. Meganur Rhaman, Associate Professor, Department of Electrical and Electronic Engineering, Ahsanullah University of Science and Technology. This thesis or any part of it has not been submitted elsewhere for the award of any degree, diploma or other qualification except for publication.

Signature of group members:

……Date: ……..……
Md. Russel Mahbub
Student ID: 15-01-05-169
Email: russelrana645@gmail.com
Mobile: 01725020036

……Date: ……
Md. Golam Muntakim
Student ID: 14-01-05-085
Email: daviddipto2015@gmail.com
Mobile: 01533295413

……Date: ……
Sharmin Akter
Student ID: 13-02-05-089
Email: sharmin027@yahoo.com
Mobile: 01622888042

DEDICATION

……..

To Almighty Allah,

Our beloved parents &

Our supervisor Sir, Md. Meganur Rhaman

Table of Contents

LIST OF FIGURES……...V

LIST OF TABLES……...IX

ACHKNOWLEDGEMENT.....IX

ABSTRACT.....1

CHAPTER 1 INTRODUCTION.....2

1.1 AIMS OF THIS RESEARCH 2

1.2 BACKGROUND OF THIS RESEARCH ON RENEWABLE ENERGY.....2

1.2.1 Bio-Energy.....3

1.2.2 Geothermal Energy.....4

1.2. 3 Hydroelectric Energy.....5

1.2.4 Hydrogen Fuel Cells.....6

1.2.5 Ocean Energy.....7

1.2.6 Wind Energy.....8

1.2.7 Solar Energy ***9***

1.2.7.1 Passive Solar Energy..... 11

1.2.7.2 Active Solar Energy 12

1.3 ADVANTAGES OF RENEWABLE ENERGY 13

1.4 DISADVANTAGES OF RENEWABLE ENERGY 14

1.5 SOLAR CELL..... 15

1.5.1 Types of Solar cell.....***15***

1.5.2 Working Principal of Solar Cell.....***18***

1.5.3 The equivalent circuit of a Solar Cell.....***20***

1.5.4 Characteristic equation..... *20*

1.5.5 Open-circuit voltage and short-circuit current..... *22*

1.5.6 Solar cell materials and efficiency..... *24*

1.6 RECENT TRENDS OF RESEARCH ON OXIDES..... 27

1.6.1 Superconducting Oxides *27*

1.6.2 Ferroelectric Oxides: *27*

1.6.3 Magnetic Oxides *29*

1.6.4 Multiferroic Oxides..... *30*

CHAPTER 2 LITERATURE REVIEW 31

2.1 INTRODUCTION TO MULTIFERROICS 31

2.2 TYPES OF MULTIFERROICS 31

2.2.1 Type I Multiferroics ***32***

2.2.2 Type II Multiferroics (Magnetic Multiferroics) *35*

2.2.3 Multiphase multiferroics *37*

2.3 BISMUTH FERRITE 37

2.3.1 History of $BiFeO_3$ *37*

2.3.2 Crystal structure of $BiFeO_3$ *38*

2.3.3 Ferroelectric properties of $BiFeO_3$ *40*

2.3.4 Magnetic order of $BiFeO_3$ *42*

2.3.5 Synthesis and Phase Diagram of $BiFeO_3$ *44*

CHAPTER 3 EXPERIMENT 46

3.1 INTRODUCTION 46

3.2 SYNTHESIS PROCEDURE 46

3.3 ANNEALING 50

3.4 MUFFLE FURNACE 51

3.5 FIELD EMISSION SCANNING ELECTRON MICROSCOPY 52

3.6 X-RAY DIFFRACTION STUDY 52

3.7 UV SPECTRA STUDY 54

3.8 PL SPECTRA STUDY 55

CHAPTER 4 RESULT & DISCUSSION 56

4.1 INTRODUCTION 56

4.2 X-RAY DIFFRACTION (XRD) 56

4.3 FESEM MICROGRAPH ANALYSIS 57

4.4 EDS DATA ANALYSIS OF THE BIFEO3 NANO PARTICLE 59

4.5 BANDGAP ENGINEERING 59

4.5.1 UV Spectrometry *60*

4.5.2 PL Spectrometry ***61***

CONCLUSION 63

SUGGESTIONS FOR FUTURE WORK 64

REFERENCE **65**

List of Figures

Figure 1.1 Biomass Power Plant in Henan Province, China…… ……..4

Figure 1.2 Geothermal Power plant (flash steam, combined cycle) in Icela……5

Figure 1.3 "The Sayano-Shushenskaya Dam" Hydroelectric Power Plant in Rus…….6

Figure 1.4 Compressed Hydrogen used in a Car……7

Figure 1.5 Ocean Technology forming in Europe……..8

Figure 1.6 Wind power stations in Xinjiang, China……...9

Figure 1.7 Solar Panel Systems on the roof of the houses…….10

Figure 1.8 Passive Solar System……11

Figure 1.9 Principle of operation of a pn junction solar cell……...19

Figure 1.10 Solar Cell equivalent circuit…….20

Figure 1.11 Solar Cell I-V Characteristic Curve…….23

Figure 1.12 Solar Panel I-V Characteristics Curves…….24

Figure 1.13 Efficiency of various research solar cells ……..25

Figure 1.14 Representation of various oxides categorized by their behavior in……26
electric and magnetic field

Figure 2.1 In "mixed" perovskites with ferroelectricity active d_0 ions……33
(green circles) and magnetic dn ions (red circles), shifts of d0
ions from oxygen octahedral (yellow plaquettes) lead to polarization

(green arrows), coexisting with magnetic order (red arrows)

Figure 2.2 n materials like $BiFeO_3$ and $PbVO_3$, the ordering of lone pairs……..34
(yellow "lobes") of Bi^{3+} and Pb^{2+} ions (orange), contributes
to the polarization (green arrow).

Figure 2.3 The "geometric" mechanism of generation of polarization in $YMnO_3$ ……..35

Figure 2.4 Different types of spin structures relevant for type-II Multiferroics……...36

Figure 2.5 Schematic illustration of a structural transition proces (a) ideal cubic……39
structure Pm-3m without tilting (a0a0a0) (b) R-3c structure tilted
along three axes with the same angle (a-a-a-); (c) Displacement of
Bi ion towards [111] direction based on R3c

Figure 2.6 **Crystal** structure of bismuth ferrite (a) in the hexagonal setting, (b)…….40
in the hexagonal setting with the distorted perovskite sub-structure
shown, and (c) viewed along the c-axis.

Figure 2.7 Schematic of crystal structure of BFO and ferroelectric polarization……41

Figure 2.8 Schematic showing different types of magnetic ordering – the last
three are types of antiferromagnetism……..42

Figure 2.9 Spin canting due to anti-symmetric exchange……43

Figure 2.10 Schematics of the 64 nm antiferromagnetic spin cycloid…….....43

Figure 2.11 Phase diagram of $Fe_2O_3$and Bi_2O_3showing bismuth ferrite with……45
undesired impurities.

Figure 3.1 Synthesis steps a) mixing raw materials into deionized water, b) formation….48
of sol, c) formation of gel, d) precursor xerogel e) ground xerogel,
f) annealed BiFeO3 powder.

Figure 3.2 Flow chart for $BiFeO_3$ powder synthesis…….49

Figure 3.3 Furnace used for annealing xerogel ……...50

Figure 3.4 Annealing cycle…….....50

Figure 3.5 Field Emission Scanning Electron Microscope (FESEM)…….....52

Figure 3.6 XRD Machine…….53

Figure 3.7 PerkinElmer UV–Vis–NIR Spectrometer Lambda 1050……54

Figure 3.8 PL spectra Machine FLS – 1000…….55

Figure 4.1 X-ray diffraction patterns of BiFeO3 particles annealed at different……..57
temperatures (a) after washing with acetic acid. (b) Magnified XRD
patterns of (102) reflection plane and (c) magnified XRD patterns
of (104) and (110)

Figure 4.2 FESEM micrographs with particle size at 700°C ……..58

Figure 4.3 EDS patterns of BFO nanoparticles …….59

Figure 4.4 $[F(R)hv]^2$ Vs eV for pure Bismuth ferrite at 700°C ……60

Figure 4.5 Intensity Vs eV for pure Bismuth ferrite from PL spectra……..61

List of Tables

Table 1.1 List of some important high temperature superconducting……...27

Table 1.2 List of some ferroelectric materials……..28

Table 1.3 List of some magnetic materials with their corresponding Curie temperatures……29

Table 4.1 Particle size and bandgap of $BiFeO_3$ by UV & PL Spectroscopy……62

ACKNOWLEDGE

In the name of Almighty Allah, the Most Gracious and the Most Merciful, Alhamdulillah, all praises to Allah for the strengths and His blessing in completing this thesis. Special appreciation goes to our supervisor**, Md. Meganur Rhaman**, Associate Professor, Department of Electrical & Electronic Engineering, Ahsanullah University of Science & Technology, for his supervision and constant support. His invaluable help of constructive comments and suggestions throughout the experimental and thesis works have contributed to the success of this research.

We are also thankful to Department of Glass & Ceramic Engineering, BUET, for their lab support & exposing us to the beauty of learning.

ABSTRACT

Solar power has evidently become the trend in renewable energy. So, enhancement of the efficiency of solar cell is very necessary in this regard. Solar cell performance can be improved by applying multiferroic thin film. Multiferroic $BiFeO_3$. (BFO) is a potential candidate for photovoltaic (PV) application. However, the efficiency of BFO based PV solar cells is reportedly still too low (less than 2%) to be used for practical applications. In this context, BFO nanoparticles were precisely synthesized using the sol-gel method at 700^0 C. Field Emission Scanning Electron Microscopy was carried out to study grain morphology of synthesized nanoparticles. The average particle size estimated from the SEM micrographs was found to be greater than the crystallite size measured from XRD analysis. An UV-Vis NIR Spectrophotometer was used to measure diffuse reflectance and a PL Spectrophotometer was used to analyze the optical properties. Bandgap E_g was calculated from both of these Spectrometries. The value of bandgap E_g from UV and PL Spectrometry were denoted to be 1.92 eV and 2.06 eV respectively.

CHAPTER 1

INTRODUCTION

1.1 Aims of this Research

The main aims of this research include:

(I) To synthesize $BiFeO_3$ nanoparticles at relatively low temperature via a soft chemistry route using simple and easily available raw materials as well as substrates.

(II) To examine microstructure and analyze particle size of synthesized BiFeO3 nanoparticles.

(III) To analyze the bandgap and other properties of pure BiFeO3 by different Spectrometries.

1.2 Background of this Research on Renewable Energy

Renewable energy, often referred to as 'Clean Energy', comes from natural sources or processes that are constantly replenished. For example, sunlight or wind keep shining and blowing, even if their availability depends on time and weather.

While renewable energy is often thought of as a new technology, harnessing nature's power has been used for heating, transportation, lighting, and more. Wind has powered boats to sail the seas and windmills to grind grain. The sun has provided warmth during the day and helped kindle fires to last into the evening. But over the past 500 years or so, humans increasingly turned to cheaper, dirtier energy sources such as coal and fracked gas.

Now that we have increasingly innovative and less-expensive ways to capture and retain wind and solar energy, renewables are becoming a more important power source, accounting for more than one-eighth of U.S. generation. At the national level, at least 30 nations around the world already have renewable energy contributing more than 20 percent of energy supply [1].

National renewable energy markets are projected to continue to grow strongly in the coming decade and beyond. Some places and at least two countries, Iceland and Norway generate all their electricity using renewable energy already, and many other countries have the set a goal to reach 100% renewable energy in the future. Renewable energy systems are rapidly becoming more efficient and cheaper and their share of total energy consumption is increasing.

Just as there are many natural sources of energy, there are many renewable energy technologies. Most of these renewable energies depend in one way or another on sunlight. In this modern era, mostly used renewable energies in the world are as follow:

- Bioenergy
- Geothermal
- Hydroelectric
- Hydrogen Fuel Cells
- Ocean Energy
- Wind Energy
- Solar Energy

1.2.1 Bio-Energy

This is a type of renewable energy derived from biomass to create heat and electricity (or to produce liquid fuels used for transportation, like ethanol and biodiesel). Biomass refers to any organic matter coming from recently living plants or animals. Even though bioenergy generates about the same amount of carbon dioxide as fossil fuels, the replacement plants grown as biomass remove an equal amount of CO_2 from the atmosphere, keeping the environmental impact relatively neutral. There are a variety of systems used to generate this type of electricity, ranging from directly burning biomass to capturing and using methane gas produced by the natural decomposition of organic material. Figure 1.1 shows a Biomass Power Plant in Henan Province, China.



Figure 1.1: Biomass Power Plant in Henan Province, China.

1.2.2 Geothermal Energy

Geothermal energy, as the name implies, is derived from the heat of the earth itself. This heat can be sourced close to the surface or from heated rock and reservoirs of hot water miles beneath our feet. Geothermal power plants harness these heat sources to generate electricity. Geothermal power is considered to be a sustainable, renewable source of energy because the heat extraction is small compared with the Earth's heat content [2]. Figure 1.2 shows a Geothermal power plant (flash steam, combined cycle) in Iceland.



Figure 1.2: Geothermal Power plant (flash steam, combined cycle) in Iceland.

1.2. 3 Hydroelectric Energy

The most familiar type of hydroelectric power is generated by a system in which dams are constructed to store water in a reservoir. When released, the water flows through turbines to produce electricity. This is known as "pumped-storage hydropower". Water is cycled between lower and upper reservoirs to control electricity generation between times of low and peak demand. Another type, called "run-of-river hydropower," funnels a portion of river flow through a channel and does not require a dam. Hydropower plants can range in size from massive projects like the Hoover Dam to micro-hydroelectric power systems. Figure 1.3 shows "The Sayano-Shushenskaya Dam" Hydroelectric Power Plant located on the Yenisei River, near Sayanogorsk in Khakassia, Russia.



Figure 1.3: "The Sayano-Shushenskaya Dam" Hydroelectric Power Plant in Russia.

1.2.4 Hydrogen Fuel Cells

A fuel cell is an electrochemical cell that converts the chemical energy of a fuel (often hydrogen) and an oxidizing agent (often oxygen) [3]. Hydrogen is the simplest (comprised of one proton and one electron) and most abundant element in the universe, yet it does not occur naturally as a gas on earth. Instead, it is found in organic compounds (hydrocarbons such as gasoline, natural gas, methanol and propane) and water (H_2O). Hydrogen can also be produced under certain conditions by some algae and bacteria using sunlight as an energy source. Hydrogen is high in energy, yet produces little or no pollution when burned. Hydrogen fuel cells convert the potential chemical energy of hydrogen into electricity, with pure water and heat as the only byproducts. However, practical and widespread commercialization of these fuel cells will likely be limited until costs come down and durability improves. Figure 1.4 shows Hydrogen Fuel Cells used in a car.



Figure 1.4: Compressed Hydrogen used in a Car

1.2.5 Ocean Energy

The ocean can produce two types of energy: thermal energy from the sun's heat, and mechanical energy from the tides and waves. Oceans cover more than 70% of Earth's surface, making them the world's largest solar collectors. The sun's heat warms the surface water a lot more than the deep ocean water, and this temperature difference creates thermal energy. Just a small portion of the heat trapped in the ocean could power the world.



Figure 1.5: Ocean Technology forming in Europe

Ocean mechanical energy harnesses the ebb and flow of tides caused by the rotation of the earth and the gravitational influence of the moon. Energy from wind-driven waves can also be converted and used to cut business electricity costs. There are also lesser-developed technologies that leverage ocean currents, ocean winds and salinity gradients as sources of power conversion.

1.2.6 Wind Energy

Wind can be considered a form of solar energy because winds are caused by the uneven heating and cooling of the atmosphere by the sun (as well as the rotation of the earth and other topographical factors). Wind flow can be captured by turbines and converted into electricity. Figure 1.6 shows the Wind power stations in Xinjiang, China. On a smaller scale, windmills are still used today to pump water on farms. Wind is caused by the uneven heating of the atmosphere by the sun, variations in the earth's surface, and rotation of the earth. Mountains,

bodies of water, and vegetation all influence wind flow patterns. Wind turbines convert the energy in wind to electricity by rotating propeller-like blades around a rotor. The rotor turns the drive shaft, which turns an electric generator. Three key factors affect the amount of energy a turbine can harness from the wind: wind speed, air density, and swept area.



Figure 1.6: Wind Power Stations in Xinjiang, China

1.2.7 Solar Energy

Except for geothermal and hydrogen, the sun plays a significant role in each of the other types of renewable energy listed here. The most direct use of this renewable energy source, however, is achieved by capturing the sun's energy directly. A variety of solar energy technologies are used to convert the sun's energy and light into heat, illumination, hot water, electricity and (paradoxically) cooling systems for businesses and industry. Photovoltaic (PV) systems use solar cells to convert sunlight into electricity. Solar hot water systems can be used

to heat buildings by circulating water through flat-plate solar collectors. The sun’s heat can be concentrated by mirror-covered dishes that are focused to boil water in a conventional steam generator to produce electricity. Commercial and industrial buildings can also leverage the sun's power for larger-scale needs such as ventilation, heating and cooling. Finally, thoughtful architectural designs can passively take advantage of the sun as a source of light and heating/cooling.

The total solar energy absorbed by Earth's atmosphere, oceans and land masses is approximately 3,850,000 exajoules (EJ) per year. In 2002, this was more energy in one hour than the world used in one year [4]. Humans can do solar photovoltaic in the desert. Solar radiation on Earth is very large. About 40 minutes of solar radiation on Earth, it can suffice the consumption of the energy for all human for one year. Nowadays, human built many solar photovoltaic plants to generate electricity, and many people are setting solar cells on the roof to generate electricity for their daily consumption. Figure 1.7 shows Solar Panel Systems on the roof of the houses in Italy.



Figure 1.7: Solar Panel Systems on the roof of the houses

There are usually two "types" of solar energy and they are defined most simply by the way they're used. These are:

1. Passive Solar Energy
2. Active Solar Energy

1.2.7.1 Passive Solar Energy

Passive Solar Energy is the use of strategically oriented walls, windows, and architectural features that are designed to absorb and deflect the sun's energy without the use of any mechanical or electrical devices. When sunlight strikes a building, the building materials can reflect, transmit, or absorb the solar radiation. In addition, the heat produced by the sun causes air movement that can be predictable in designed spaces. These basic responses to solar heat lead to design elements, material choices and placements that can provide heating and cooling effects in a home. Unlike active solar heating systems, passive systems are simple and do not involve substantial use of mechanical and electrical devices, such as pumps, fans, or electrical controls to move the solar energy. Figure 1.8 is a simple model of a home designed for passive solar energy.

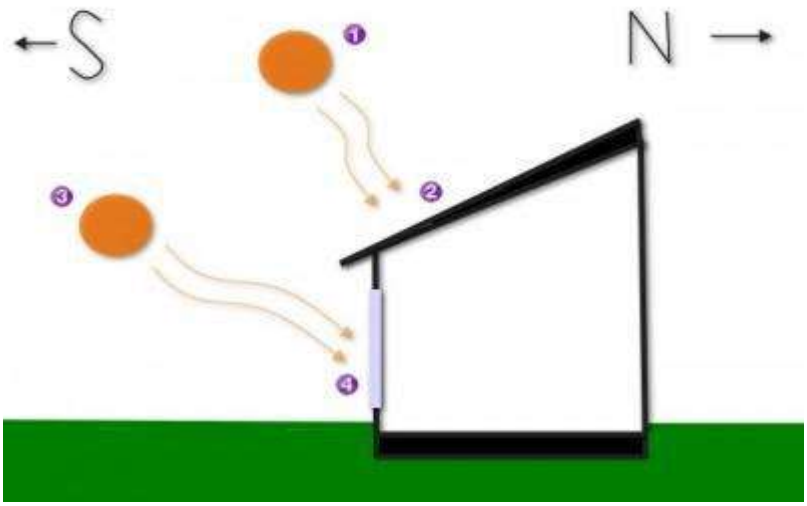


Figure 1.8: Passive Solar System

Passive solar heating of figure 1.8 is a generic image of the side of a house that is strategically oriented to absorb the sun's heat in the winter and deflect the sun's heat in the summer. The working principals are as follow:

1. The sun labeled in Figure 1.8 is an example of a summer sun in the Northern Hemisphere because it is higher in the sky when oriented with solar south.
2. The rays of the summer sun are absorbed or reflected off the specially designed roof of the house which keeps the house cooler in the summer.
3. The winter sun is closer to the horizon.
4. The strategically placed window of the house is designed to let in the heat of the winter sun, which will keep the house warmer during the winter and hopefully result in lower energy usage to heat home.

In passive solar heating, the sun's rays are not converted into electricity.

1.2.7.2 Active Solar Energy

Active Solar Energy uses an active electrical device to power the solar energy system, such as a water pump or an electrical power control box. Because of this requirement, an active solar energy system requires extra power, besides the sun, to operate and maximize the efficiency of the system.

Active solar systems come with many advantages. The obvious advantage of the active system is that the outside power source increases the efficiency of the system. Another advantage is that it makes controlling the system much easier by offering controls to turn the machine on and off, and also to adjust specific options of the machines, such as temperature. Active solar energy systems are cost-effective in certain conditions. One of them is its use If it is used at a large scale to supply energy to a full house then it is cost-effective as there is no need to worry about its maintenance. It is comparatively more useful than fossil fuels. It emits zero carbon in the environment so it is a safeguard for health issues. It requires only one-time heavy investment for a lifetime solar energy. It hardly needs extra charges on its maintenance.

In case of its use only even during daylight is a good supplement of electricity. For a short time of inconvenience can be replaced by a sort of backup energy. This backup energy could be fossil fuels or electricity receiving through power houses. Where it reduces the use of backup electricity source there it shows a great reduction in billing amount. Active solar energy system can be designed cost-effectively by using other liquid still in search as to what is more suitable for a quantitative and qualitative production of electricity. Active solar energy system does not produce greenhouse gases and give a pollution free environment. There are various forms of "Active Solar Energy". Among those, Photovoltaic Cells (PV) are being used in wide range in the rest of the world.

1.3 Advantages of Renewable energy

Using renewable energy over fossil fuels has a number of advantages. Here are some of the top benefits of going green:

- **Renewable energy won't run out**

Renewable energy technologies use resources straight from the environment to generate power. These energy sources include sunshine, wind, tides, and biomass, to name some of the more popular options. Renewable resources won't run out, which cannot be said for many types of fossil fuels – as we use fossil fuel resources, they will be increasingly difficult to obtain, likely driving up both the cost and environmental impact of extraction.

- **Maintenance requirements are lower**

In most cases, renewable energy technologies require less overall maintenance than generators that use traditional fuel sources. This is because generating technology like solar panels and wind turbines either have few or no moving parts and don't rely on flammable, combustible fuel sources to operate. Fewer maintenance requirements translate to more time and money saved.

- **Renewable Energy save money**

Using renewable energy can help you save money long term. Not only will you save on maintenance costs, but on operating costs as well. When you're using a technology that generates power from the sun, wind, steam, or natural processes, you don't have to pay to refuel. The amount of money you will save using renewable energy can vary depending on a number of factors, including the technology itself. In most cases, transitioning to renewable energy means anywhere from hundreds to thousands of dollars in savings.

- **Renewable energy has numerous health and environmental benefits**

Renewable energy generation sources emit little to no greenhouse gases or pollutants into the air. This means a smaller carbon footprint and an overall positive impact on the natural environment. During the combustion process, fossil fuels emit high amounts of greenhouse gases, which have been proven to exacerbate the rise of global temperatures and frequency of extreme weather events.

The use of fossil fuels not only emits greenhouse gases but other harmful pollutants as well that lead to respiratory and cardiac health issues. With renewable energy, you're helping decrease the prevalence of these pollutants and contributing to an overall healthier atmosphere.

- **Renewables lower reliance on foreign energy sources**

With renewable energy technologies, you can produce energy locally. The more renewable energy you're using for your power needs, the less you'll rely on imported energy, and the more you'll contribute to U.S. energy independence as a whole.

1.4 Disadvantages of Renewable Energy

Renewable energy has many benefits, but it's not always sunny when it comes to renewable energy. Here are some disadvantages to using renewables over traditional fuel sources.

- **Higher upfront cost**

While you can save money by using renewable energy, the technologies are typically more expensive upfront than traditional energy generators. To combat this, there are often

financial incentives, such as tax credits and rebates, available to help alleviate your initial costs of renewable technology.

- **Intermittency**

Though renewable energy resources are available around the world, many of these resources aren't available 24/7, year-round. Some days may be windier than others, the sun doesn't shine at night, and droughts may occur for periods of time. There can be unpredictable weather events that disrupt these technologies. Fossil fuels are not intermittent and can be turned on or off at any given time.

- **Storage capabilities**

Because of the intermittency of some renewable energy sources, there's a high need for energy storage. While there are storage technologies available today, they can be expensive, especially for large-scale renewable energy plants. It's worth noting that energy storage capacity is growing as the technology progresses, and batteries are becoming more affordable as time goes on.

1.5 Solar Cell

A solar cell, or photovoltaic cell, is an electrical device that converts the energy of light directly into electricity by the photovoltaic effect, which is a physical and chemical phenomenon. It is a form of photoelectric cell, defined as a device whose electrical characteristics, such as current, voltage, or resistance, vary when exposed to light. Individual solar cell devices can be combined to form modules, otherwise known as solar panels. In basic terms a single junction silicon solar cell can produce a maximum open-circuit voltage of approximately 0.5 to 0.6 volts.

1.5.1 Types of Solar Cell

Photovoltaic cells or PV cells can be manufactured in many different ways and from a variety of different materials. Despite this difference, they all perform the same task of harvesting solar energy and converting it to useful electricity. The most common material for

solar panel construction is silicon which has semiconducting properties. Several of these solar cells are required to construct a solar panel and many panels make up a photovoltaic array.

There are several types of PV cell technologies which are being constructed in the world. These are:

• Monocrystalline Silicon Cell

• Polycrystalline Silicon Cell

• Thin Film Cells

• Multi-Junction

• Nano-Crystalline Solar Cells

• Organic Solar Cells

Monocrystalline Silicon Cell

The first commercially available solar cells were made from monocrystalline silicon, which is an extremely pure form of silicon. To produce these, a seed crystal is pulled out of a mass of molten silicon creating a cylindrical ingot with a single, continuous, crystal lattice structure. This crystal is then mechanically sawn into thin wafers, polished and doped to create the required p-n junction. After an anti-reflective coating and the front and rear metal contacts are added, the cell is finally wired and packaged alongside many other cells into a full solar panel. Monocrystalline silicon cells are highly efficient, but their manufacturing process is slow and labor intensive, making them more expensive than their polycrystalline or thin film counterparts.

Polycrystalline Silicon Cell

Instead of a single uniform crystal structure, polycrystalline (or multi-crystalline) cells contain many small grains of crystals. They can be made by simply casting a cube-shaped ingot from molten silicon, then sawn and packaged similar to monocrystalline cells. Another method

known as edge-defined film-fed growth (EFG) involves drawing a thin ribbon of polycrystalline silicon from a mass of molten silicon. A cheaper but less efficient alternative, polycrystalline silicon PV cells dominate the world market, representing about 70% of global PV production in 2015.

Thin Film Cells

Although crystalline PV cells dominate the market, cells can also be made from thin films by making them much more flexible and durable. One type of thin film PV cell is amorphous silicon (a-Si) which is produced by depositing thin layers of silicon on to a glass substrate. The result is a very thin and flexible cell which uses less than 1% of the silicon needed for a crystalline cell [3]. Due to this reduction in raw material and a less energy intensive manufacturing process, amorphous silicon cells are much cheaper to produce. Their efficiency, however, is greatly reduced because the silicon atoms are much less ordered than in their crystalline forms leaving 'dangling bonds' that combine with other elements making them electrically inactive. These cells also suffer from a 20% drop in efficiency within the first few months of operation before stabilizing, and are therefore sold with power ratings based on their degraded output.

Other types of thin film cells include copper indium gallium diselenide (CIGS) and cadmium telluride (CdTe). These cell technologies offer higher efficiencies than amorphous silicon, but contain rare and toxic elements including cadmium which requires extra precautions during manufacture and eventual recycling.

Multi-Junction

The majority of PV cells, including those discussed above, contain only one p-n junction of semiconductor material which converts energy from one discreet portion of the solar spectrum into useful electricity. Multi-junction cells have 2 or more junctions layered on top of

each other, allowing energy to be collected from multiple portions of the spectrum. Light that is not absorbed by the first layer will travel through and interact with subsequent layers. Multi-junction cells are produced in the same way as gallium arsenide cells—slowly depositing layers of material onto a single crystal base,

making them very expensive to produce, and only commercially viable in concentrated PV systems and space applications.

Nano-Crystalline Solar Cells

Nano-crystalline TiO_2 solar cells chemical energy is a newly developed, is that it costs cheap and simple process and a stable performance. The optical efficiency of 10% or more stable, production cost of silicon solar cells is only 1 / 5 ~ 1 / 10. Life can reach more than 20 years. Research and development of such batteries just started in the near future will gradually onto the market.

Organic solar cells

Organic solar cells, organic materials that constitute the core part of the solar cells. We are not familiar with organic solar cells, which is reasonable in the matter. Now in mass production of solar cells, more than 95% of silicon, while the remaining less than 5% is made by other inorganic materials.

1.5.2 Working Principle of Solar Cell

The most commonly known solar cell is configured as a large-area p–n junction made from silicon. Other possible solar cell types are organic solar cells, dye sensitized solar cells, perovskite solar cells, quantum dot solar cells etc. The illuminated side of a solar cell generally has a transparent conducting film for allowing light to enter into active material and to collect the generated charge carriers. Typically, films with high transmittance and high electrical conductance such as indium tin oxide, conducting polymers or conducting nanowire networks are used for the purpose. The solar cell works in several steps as follow:

• At first, Photons in sunlight hit the solar panel and are absorbed by semiconducting materials, such as silicon.

• After that, Electrons are excited from their current molecular/atomic orbital. Once excited an electron can either dissipate the energy as heat and return to its orbital or travel through the cell until it reaches an electrode. Current flows through the material to cancel the potential and this electricity is captured. The chemical bonds of the material are vital for this process to work, and usually silicon is used in two layers, one layer being doped with boron, the other phosphorus. These layers have different chemical electric charges and subsequently both drive and direct the current of electrons.

• An array of solar cells converts solar energy into a usable amount of direct current (DC) electricity.

• An inverter can convert the power to alternating current (AC).

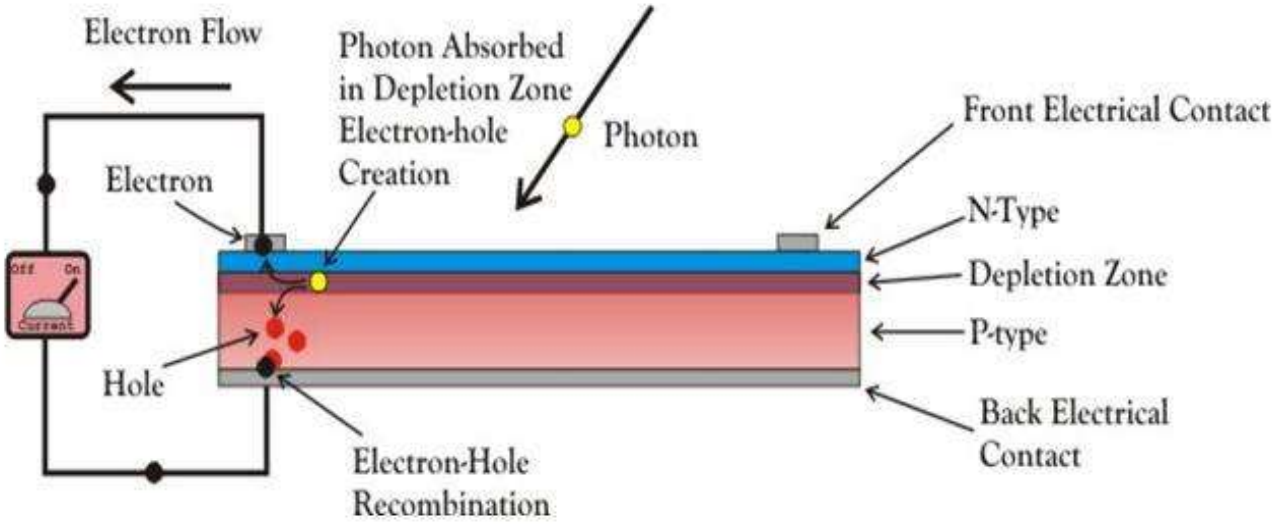


Figure 1.9: Principle of operation of a pn junction solar cell. Radiation is absorbed in the depletion region and produces electrons and holes. These are separated by the built-in potential. Depending on the wavelength and the thickness different parts of the device can absorb different regions of the solar spectrum. [5]

1.5.3 The equivalent circuit of a Solar Cell

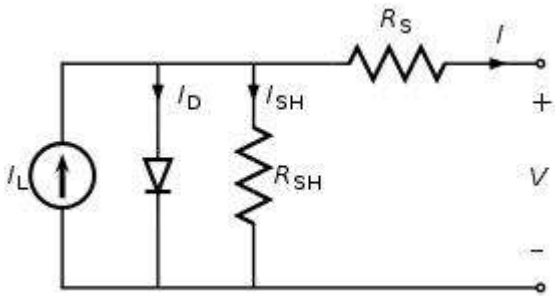


Figure 1.10: Solar Cell equivalent circuit.

To understand the electronic behavior of a solar cell, it is useful to create a model which is electrically equivalent, and is based on discrete electrical components whose behavior is well known. An ideal solar cell may be modelled by a

current source in parallel with a diode; in practice no solar cell is ideal, so a shunt resistance and a series resistance component are added to the model. The resulting equivalent circuit of a solar cell is shown on the left. Also shown, on the right, is the schematic representation of a solar cell for use in circuit diagrams.

1.5.4 Characteristic equation

From the equivalent circuit it is evident that the current produced by the solar cell is equal to that produced by the current source, minus that which flows through the diode, minus that which flows through the shunt resistor:

……. (1)

where

I = output current (amperes)

I_L = photo generated current (amperes)

I_D = diode current (amperes)

I_{SH} = shunt current (amperes).

The current through these elements is governed by the voltage across them:

= + ... (2)

Where,

V_j = voltage across both diode and resistor RSH (volts)

V = voltage across the output terminals (volts)

I = output current (amperes)

R_S = series resistance (Ω).

By the Shockley diode equation, the current diverted through the diode is:

= 0 {exp [ ] − 1}..... (3)

Where,

I_0 = reverse saturation current (amperes)

n = diode ideality factor (1 for an ideal diode)

q = elementary charge

k = Boltzmann's constant

T = absolute temperature

At 25°C,

By Ohm's law, the current diverted through the shunt resistor is:

=

—— ..... (4)

R_{SH} = shunt resistance (Ω).

Substituting equation (1), (2) and (3) into the equation (1) produces the characteristic equation of a solar cell, which relates solar cell parameters to the output current and voltage:

$$I = I_L - I_0 \left\{ \exp\left[\frac{q(V + IR_S)}{nkT} \right] - 1 \right\} - \frac{V + IR_S}{R_{SH}}.$$

An alternative derivation produces an equation similar in appearance, but with V on the left-hand side. The two alternatives are identities; that is, they yield precisely the same results.

In principle, given a particular operating voltage V the equation may be solved to determine the operating current I at that voltage. However, because the equation involves I on both sides in a transcendental function the equation has no general analytical solution. However, even without a solution it is physically instructive. Furthermore, it is easily solved using numerical methods. (A general analytical solution to the equation is possible using Lambert's W function, but since Lambert's W generally itself must be solved numerically this is a technicality.)

Since the parameters I_0, n, R_S, and R_{SH} cannot be measured directly, the most common application of the characteristic equation is nonlinear regression to extract the values of these parameters on the basis of their combined effect on solar cell behavior.

1.5.5 Open-circuit voltage and short-circuit current

When the cell is operated at open circuit, I = 0 and the voltage across the output terminals is defined as the open-circuit voltage. Assuming the shunt resistance is high enough to neglect the final term of the characteristic equation, the open-circuit voltage V_{OC} is:

$$V_{OC} \approx \frac{kT}{q} \ln\left(\frac{I_L}{I_0} + 1 \right).$$

Similarly, when the cell is operated at short circuit, V = 0 and the current I through the terminals is defined as the short-circuit current.

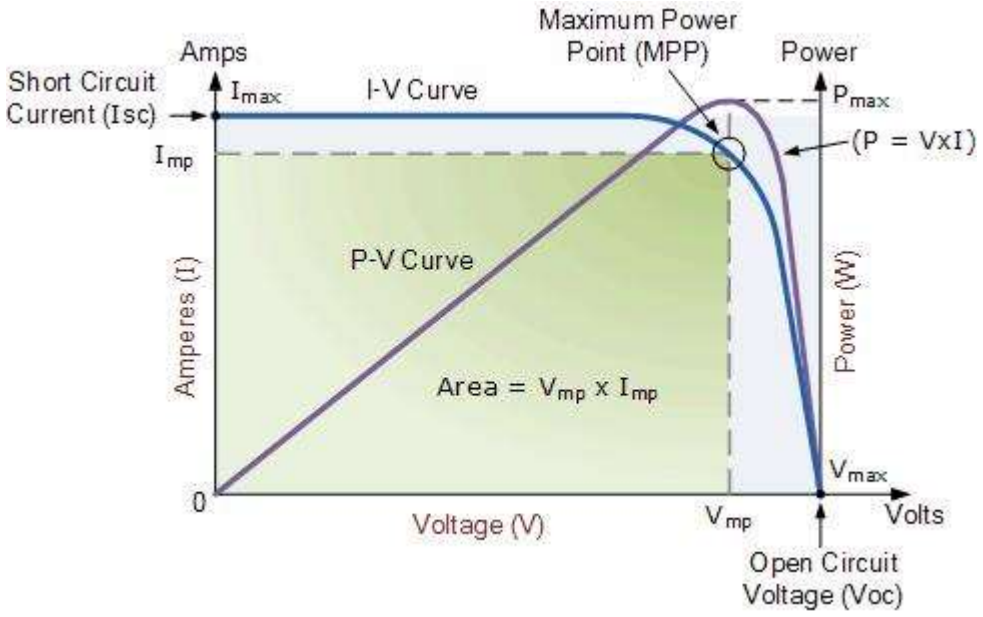


Fig1.11: Solar Cell I-V Characteristic Curve

Figure 1.11: The current-voltage (I-V) characteristics of a typical silicon PV cell operating under normal conditions. The power delivered by a solar cell is the product of current and voltage (I x V). If the multiplication is done, point for point, for all voltages from short-circuit to open-circuit conditions, the power curve above is obtained for a given radiation level.

With the solar cell open-circuited, that is not connected to any load, the current will be at its minimum (zero) and the voltage across the cell is at its maximum, known as the solar cells open circuit voltage, or Voc. At the other extreme, when the solar cell is short circuited, that is the positive and negative leads connected together, the voltage across the cell is at its minimum (zero) but the current flowing out of the cell reaches its maximum, known as the solar cells short circuit current, or I_{sc}. Then the span of the solar cell I-V characteristics curve ranges from the short circuit current (I_{sc}) at zero output volts, to zero current at the full open circuit voltage (V_{oc}). In other words, the maximum voltage available from a cell is at open circuit, and the maximum current at closed circuit. Of course, neither of these two conditions generates any

electrical power, but there must be a point somewhere in between were the solar cell generates maximum power. Figure 1.12 shows solar panel I-V characteristics curves.

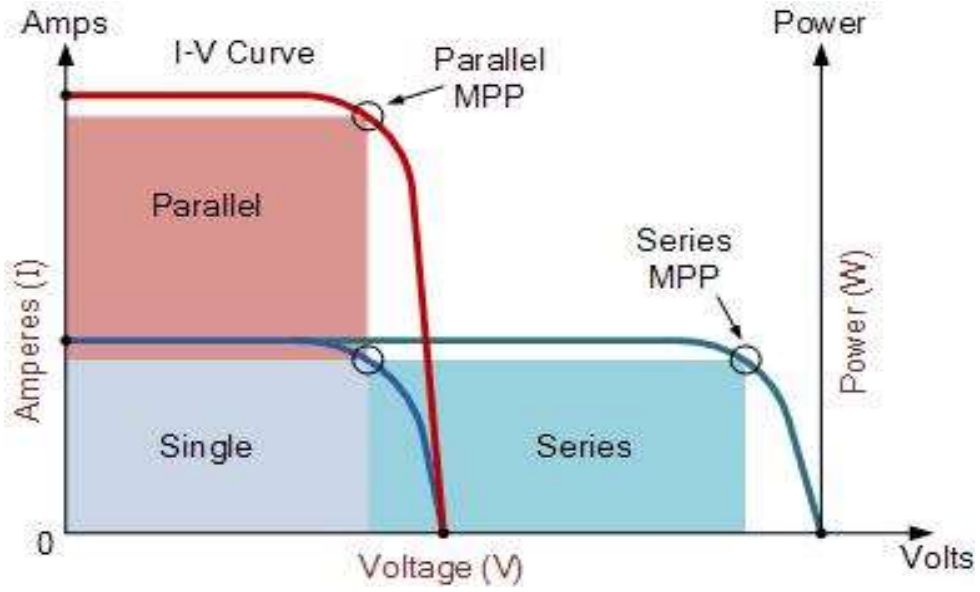


Figure 1.12: Solar Panel I-V Characteristics Curves

1.5.6 Solar cell materials and efficiency

Conventional solar cells are made of Si single crystal and have an efficiency of around 22-24%, while polycrystalline Si cells have an efficiency of 18%. A schematic representation of such a cell is shown in figure 1.13. Polycrystalline solar cells are cheaper to manufacture but have a lower efficiency since the microstructure introduces defects in the material that can trap carriers. Amorphous solar cells have an even lower efficiency but can be grown directly on glass substrates by techniques like sputtering so that the overall cost of manufacturing is lowered. There are also design improvements in the solar cell that can enhance the efficiency.

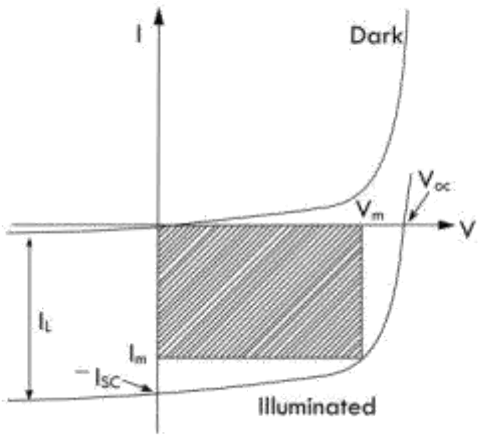


Figure 1.13: I-V curve for a solar cell with maximum power indicated by the shaded area. The corresponding voltage and current are Vm and Im. The value depends on the external load applied. Adapted from Physics of semiconductor devices - S.M. Sze

Typical solar cells are made of the same material so that the pn junction is a homo-junction. Some solar cell materials and their efficiencies are summarized in table 1. A comprehensive state of current research in different solar cell technologies and their efficiency is available in figure 1.14. Heterojunction solar cells are also possible and they have the advantage of minimizing ab-sorption in regions other than the depletion region, but overall cost increases because of the use of different materials and the tight processing conditions needed to produce defect free interfaces.

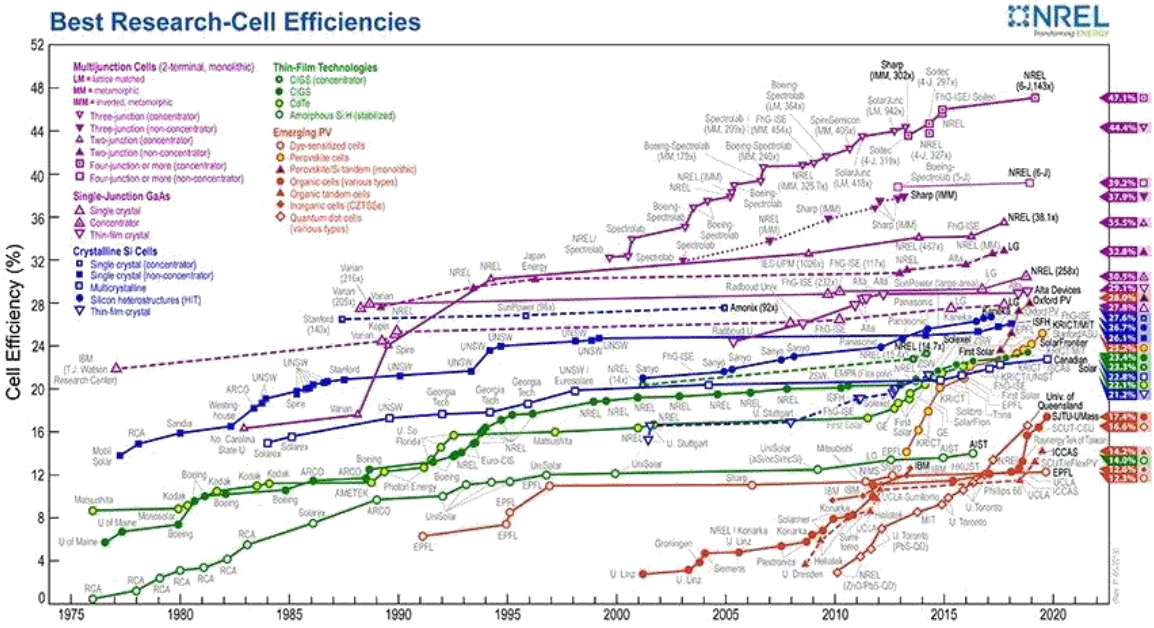


Figure 1.14: Efficiency of various research solar cells. [6]

The National Renewable Energy Laboratory (NREL) maintains a plot of compiled values of highest confirmed conversion efficiencies for research cells, from 1976 to the present, for a range of photovoltaic technologies. Devices included in this plot of the current state of the art have efficiencies that are confirmed by independent, recognized test labs (e.g., NREL, AIST, Fraunhofer) and are reported on a standardized basis. The measurements for new entries must be with respect to Standard Test or Reporting Conditions (STC) as defined by the global reference spectrum for flat-plate devices and the direct reference spectrum for concentrator devices as listed in standards IEC 60904-3 edition 2 or ASTM G173. The reference temperature is 25°C and the area is the cell total area or the area defined by an aperture. Cell efficiency results are provided within different families of semiconductors. Some 26 different subcategories are indicated by distinctive colored symbols. The most recent world record for each technology is highlighted along the right edge in a flag that contains the efficiency and the symbol of the technology. The company or group that fabricated the device for each most-recent record is bolded on the plot.

1.6 Recent trends of research on oxides

Since very beginning metal oxides have been the most focused study from application as well as fundamental physics point of view. Their properties are strongly related to their structure, and variety of interesting physics has been witnessed on varying the external stimuli such as temperature and pressure. These properties have not only opened the door for various applications but also a better understanding of the physics involved. Some of the interesting properties include superconductivity, ferroelectricity, magnetism and multiferroicity.

1.6.1 Superconducting Oxides

Until Bednorz & Muller reported superconductivity (1986) at ~23K in an oxide based compound, the superconducting phenomenon was considered only as low (Helium) temperature business and hence limited applications. Soon other oxide based superconductors were discovered whose superconducting transition temperature was much above that predicted by BCS theory for conventional superconductors, hence termed high temperature superconductor (HTS). Some of the HTS are listed in the chronological order of transition temperature in table-1.1 [7].

Table 1.1: List of some important high temperature superconducting materials

Material	T_c (K)
$YBa_2Cu_3O_7$ (YBCO)	90
$Bi_2Sr_2Ca1\text{-}xCu_nO_{2n}+4$ (BSSCCO)	122
$TiBa_2Ca_n\text{-}_1Cu_nO_{2n}+4$(TBSSCO)	127
$TiBa_2Ca_n$-1CunO2n+3(TBSSCO)	122
$HgBa_2Ca_n$-1CunO2n+2	128

1.6.2 Ferroelectric Oxides

Ceramic oxides with non-centrosymmetric perovskite structure generally show ferroelectricity. These oxides are used in bulk and thin film form for various applications. The ferroelectric properties of these oxides make them for use as non-volatile memory. The piezoelectric property of these materials enhances their use in actuators and ultrasound imaging. The high dielectric constant of these materials facilitates there use in capacitors and memory devices. The ferroelectric, piezoelectric and dielectric properties of the material are enhanced by doping the material with suitable dopants [8]. Now the current trend is to synthesize the ferroelectric oxides which give above properties at room temperature, for their applications. These oxides include BaTiO3, CaTiO3, PbTiO3 and SrTiO3 along with suitable dopants. Due to toxicity and high volatility of Lead (Pb), now a day there is awareness for synthesizing the lead free ceramic oxides for ferroelectric application. The different ferroelectric oxides with their dielectric constant values are given in table 1.2.

Table 1.2: List of some ferroelectric materials

Materials	Dielectric constant
$SrTiO_3$	310
$Ba_{1-x}Sr_xTiO_3$	500
$BaTiO_3$	1250–10,000 (20–120°C)
$CaTiO_3$	300
$(La,Nb,Zr,Ti)PbO_3$	500–6000

1.6.3 Magnetic Oxides

Magnetic materials have become an integral part of our day-to-day life, owing to their various applications in different areas. Generally magnetic materials can be classified in soft and hard form, from the view point of magnetic property. The soft magnets are the magnets having low coercivity in the hysteresis loop and vice versa. The magnetic oxides are generally soft magnets. Due to low coercivity they are used into an alternating magnetic field. They show excellent magnetic property in high frequency as compared with metal magnetic materials. They show high electrical resistivity and smaller eddy current loss. These soft magnetic oxides generally include ferrites, magnetites and cobaltite. Generally soft ferrites exist in two types of structures, i.e., spinel type and garnate type. They show the properties like high Curie temperature, high permeability and high stability. Transition metals like iron (Fe), cobalt (Co) manganese (Mn) and nickel (Ni) combining with oxygen and other various magnetic oxides with their magnetic flux density and Curie temperature values are listed in the table 1.3.

Table 1.3: List of some magnetic materials with their corresponding Curie temperatures.

Chemical formula	Magnetic flux density (Tesla) at room temperature	Ferromagnetic Curie temperature(T_c) in K
$MnFe_2O_4$	400	570
$CoFe_2O_4$	480	790
$NiFe_2O_4$	270	860
Y_3FeO_{12}	135	550
$Ba_3Co_2Fe_{24}O_{41}$	270	683

1.6.4 Multiferroic Oxides

These oxides have the unique properties of both ferromagnetism and ferroelectricity in a single crystal. This opens broader applications in transducers, magnetic field sensors and information storage industry. These include $BiFeO_3$, $BiMnO_3$, $TbMnO_3$, $TbMn_2O_5$, $YMnO_3$ and $LuFeO_4$. Among these oxides $BiFeO_3$ (BFO) is the only material which gives ferroelectricity and antiferromagnetism at room temperature [9].

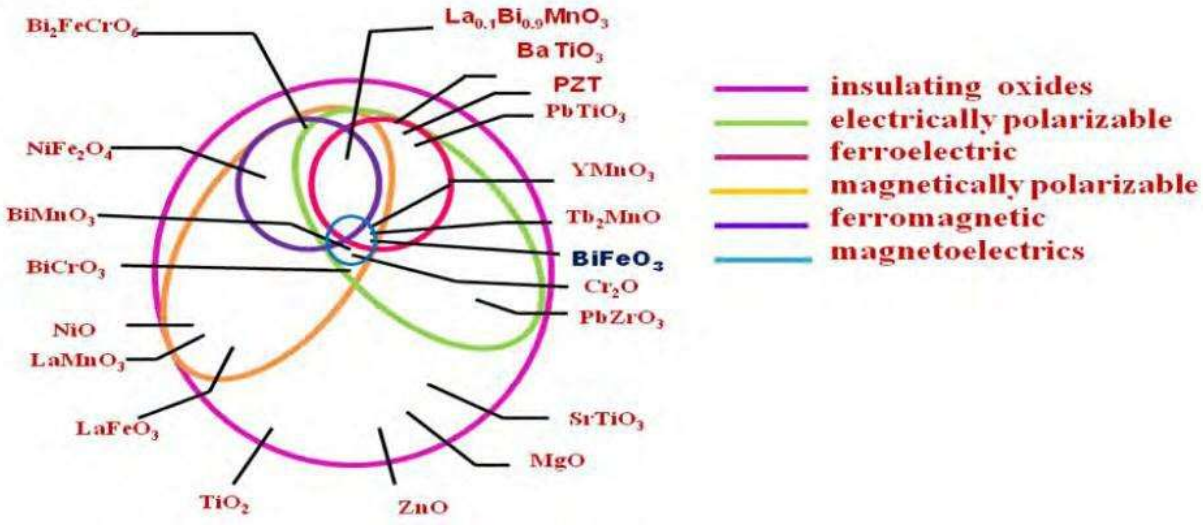


Figure 1.15: Representation of various oxides categorized by their behavior in electric and magnetic field.

Due to coexistence of both ferromagnetism and ferroelectricity in the same material, it is expected to exhibit ferromagnetic & ferroelectric properties or a coupling of these two properties in a single material. This increases the current range of application and moreover interesting physics may be observed. Presently lot of research work is carried out on this particular field in different forms like bulk, powder, thin film and nanostructure.

CHAPTER 2

LITERATURE REVIEW

2.1 Introduction to Multiferroics

Multiferroics belong to a newer class of magnetoelectric materials in which Ferro/antiferromagnetic and ferroelectric properties occur simultaneously. Although a few multiferroic materials were known in early sixties they did not attract much attention owing to their small values of polarization. Recent trends in the miniaturization of devices, increased storage density of memories, faster and more efficient processes of storing and retrieving data, etc., have revived research on multiferroic materials for such applications. In recent years, the use of sophisticated experimental facilities for their preparation, state-of-the-art characterization techniques, improved theoretical background and powerful computational tools have shed more light on understanding the fundamental phenomena as well as technological hurdles of multiferroics. In this chapter, the concept of multiferroic materials is given and recent progress in the research into them is discussed.

2.2 Types of Multiferroics

The microscopic origin of magnetism is basically the same in all magnets; it is the presence of localized electrons, mostly in the partially filled d or f shells of transition metal or rare earth ions, which have corresponding localized spin, or magnetic moment. Exchange interactions between localized moments lead to magnetic order. However, the situation is different in case of ferroelectrics. There are several different microscopic origins of ferroelectricity and accordingly one can have different types of Multiferroics.

Generally, the Multiferroics are categorized in two groups: (i) type I Multiferroics and (ii) type II Multiferroics, on the basis of the origin of ferroelectricity in them.

2.2.1 Type I Multiferroics

This group of Multiferroics contains those perovskites in which ferroelectricity and ferromagnetism have different sources (cations at A-site and B-site respectively). These materials show weak magnetoelectric coupling. In these materials, ferroelectricity typically appears at higher temperatures than magnetism and they exhibit large spontaneous polarization. Examples are $BiFeO_3$ (T_c ~ 1110 K, T_N ~ 643 K, P ~ 90 μC/cm2), $YMnO_3$ (T_c FE ~ 914 K, T_N ~76 K, P ~ 6 μC/cm2). These materials have been extensively studied since 1960‟s. However, major challenge in these materials is to enhance the values of Magnetic coupling coefficient. Type I Multiferroics are further classified in many subclasses on the basis of origin of ferroelectricity.

(a) Ferroelectricity due to shifting of B-cation

Probably the best-known ferroelectrics are the perovskites like $BaTiO_3$ or $Pb(ZrTi)O_3$ (PZT). There are many magnetic materials among perovskites, and also many ferroelectrics. Theoretical studies have shown that the usual atomic-level mechanisms for ferromagnetism and ferroelectricity are quite different. Whereas for magnetism one needs partially filled d shells of a transition metal, practically all ferroelectric perovskites contain transition metal ions with an empty d shell, such as Ti^{4+}, Ta^{5+} W^{6+} Ferroelectricity in these systems is caused by the off- center shifts of the transition metal ion, which forms strong covalent bonds with one (or three) oxygens, using their empty d states. And somehow, the presence of real d electrons in d_n configurations of magnetic transition metals suppresses this process, preventing ferroelectricity in magnetic Perovskites. This so called "d_0 vsd_n problem" was one of the first to be studied theoretically at the beginning of the recent revival of multiferroics [10], and although there has been some progress, still there is no full solution of this problem [11]. The answer may well lie in the fact that this mutual exclusion is not a "theorem" but rather a matter of numbers: in most cases a magnetic d_n ion is stable in the center of its MO_6 octahedral, but there may still be the cases where it is not. One possible way around this problem may be making "mixed" perovskites with d_0 and d_n ions. However, the coupling of magnetic and ferroelectric subsystems in mixed perovskites is weak.

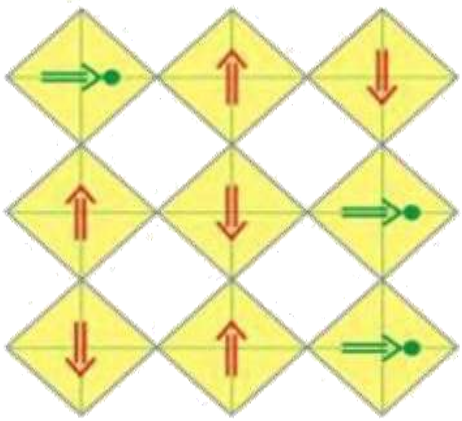


Figure 2.1: In "mixed" perovskites with ferroelectricity active d_0 ions (green circles) and magnetic dn ions (red circles), shifts of d0 ions from oxygen octahedral (yellow plaquettes) lead to polarization (green arrows), coexisting with magnetic order (red arrows).

(b) Ferroelectricity due to lone pairs

These multiferroic materials exhibit ferroelectricity due to lone pair at A-site cation. Most of Bismuth (Bi) and Lead (Pb) based perovskites show ferroelectricity due to lone pair, for example $BiFeO_3$, $BiMnO_3$, and $PbVO_3$. In these materials Bi^{3+} and Pb^{2+} have two outer 6s electrons that do not participate in chemical bonds. These electrons are called "lone pairs" or sometimes dangling bonds. Microscopically, one can explain the origin of ferroelectricity in these compounds by the ordering of these lone pairs (with certain admixture of p-orbitals) in the direction of electric field. The magnetism in these materials is originated from B-cation.

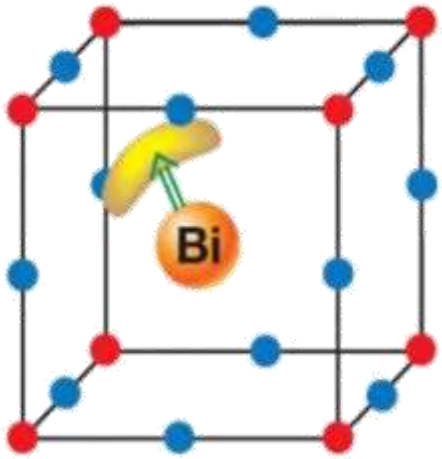


Figure 2.2: In materials like $BiFeO_3$ and $PbVO_3$, the ordering of lone pairs (yellow "lobes") of Bi^{3+} and Pb^{2+} ions (orange), contributes to the polarization (green arrow) [12]

(c) Ferroelectricity due to charge ordering

This is another group of ferroelectrics, in which the electric polarization is induced due to the non-Centro symmetry of charges. The non-Centro symmetry of charges is normally observed in transition metal compounds (especially transition metal ions with different metal states) e.g. $Pr_0.5Ca_0.5MnO_3$ or in Nickelates $RNiO_3$ [13].

(d) Geometric ferroelectricity

In this category of Multiferroics, some geometric disorder in the lattice causes ferroelectricity. For example, in case of $YMnO_3$, ferroelectricity has nothing to do with individual cations, but is caused by the tilting of practically rigid MnO_5 block with respect to Y-ions [19]. This tilting occurs just to provide closer packing, and as a result the oxygen ions moves closer to the rather small Y ions.



Figure 2.3: The "geometric" mechanism of generation of polarization in $YMnO_3$ [13] describes the tilting of a rigid MnO_5 block with a magnetic Mn remaining at the center. Because of the tilting, the Y-O bonds form dipoles (green arrows), and there appears two "up" dipoles per one "down" dipole so that the system becomes ferroelectric (and multiferroic when Mn spins order at lower temperatures).

2.2.2 Type II Multiferroics (Magnetic Multiferroics)

The materials in which the ferroelectricity is originated from magnetism and implies strong magnetoelectric coupling. However, the polarization in these materials is usually much smaller (10-2 μC/cm2). These Multiferroics are recently discovered. $TbMnO_3$ and $TbMn_2O_5$ are typical examples of these materials [14,15]. Kimura et al [14] demonstrate strong influence of magnetic field on electric polarization. In $TbMnO_3$, the polarization rotates (or "flops") by 90 degrees when a critical field is applied in a certain direction [16]. Influence of magnetic field is even stronger in case of $TbMn_2O_5$ [17]. The polarization changes sign with magnetic field. Since the discovery of these materials, a number of other type-II Multiferroics with strong magnetoelectric coupling have been discovered and studied. On the basis of mechanism of multiferroic behavior, one can divide type-II Multiferroics in two categories.

(a) Spiral Type-II Multiferroics

In this type of Multiferroics, the ferroelectricity appears in conjunction with a spiraling magnetic phase, mostly cycloid type. $TbMnO_3$, $Ni_3V_2O_6$ and $MnWO_4$ are typical examples of this type of multiferroics. Therefore, these type-II multiferroics are usually found in frustrated magnetic systems.

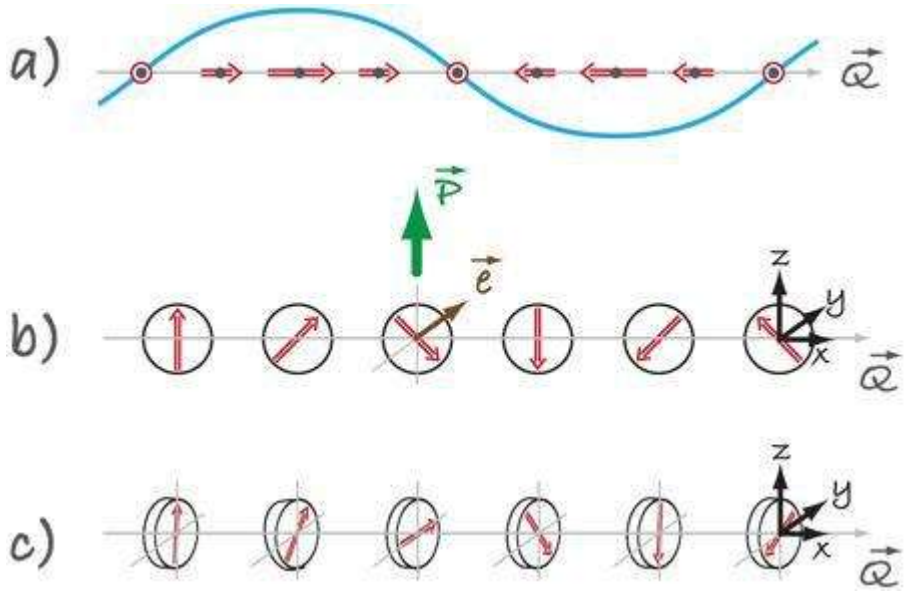


Figure 2.4: Different types of spin structures relevant for type-II Multiferroics (a) Sinusoidal spin density wave, in which spins point along one direction but vary in magnitude. This structure is centrosymmetric and consequently not ferroelectric. (b) The cycloidal spiral with the wave vector $Q = Q_x$ and spins rotating in the (x,z)-plane. It is in this case where one finds nonzero polarization, $Pz \neq 0$. (c) In a so-called "proper screw" the spins rotate in a plane perpendicular to Q. Here the inversion symmetry is broken, but most often it does not produce polarization, although in certain cases it might [49].

(b) Type-II Multiferroics with Collinear Magnetic Structures

In this group of Type-II multiferroics ferroelectricity appears in collinear magnetic structures; i.e., all magnetic moments are aligned along a particular axis without the necessary involvement of spin-orbit interaction. Polarization can appear in these materials as a consequence of exchange striction because the magnetic coupling varies with atomic positions. The simplest example of this type of multiferroics is Ca_3CoMnO_6 [18].

2.2.3 Multiphase multiferroics

The choice of single-phase materials exhibiting the coexistence of at least two ferroic orders at room temperature is quite limited. The scarcity of single phase multiferroic materials makes composite/ multiphase multiferroics an interesting alternative. Magnetoelectric multiferroic composites consist of a ferroelectric phase and ferromagnetic phase, and the coupling between the two orderings is through stress mediation. The Magnetoelectric effect is extrinsic in this case since magnetoelectric effect is not exhibited by any of the constituent phases on their own. Various constituent materials have been studied as multiferroic composite materials, such as $BaTiO3$-$CoFe_2O_4$, $BaTiO_3$-$NiFe_2O_4$, PZT-$NiFe_2O_4$, PZT-$CoFe_2O_4$, $BiFeO_3$-$CoFe_2O_4$, and $BiFeO_3$-$NiFe_2O_4$.

2.3 Bismuth Ferrite

Bi-based compounds are of main interest due to their multiferroic behavior. There are many Bi- based perovskite compounds in which B-site is accommodated by transition metals e.g. $BiFeO_3$, $BiMnO_3$, $BiCrO_3$ etc. These compounds fall into the category of "Type-I multiferroics". Ferroelectricity originates from the alignment of lone pair of Bi^{3+} ion and magnetism comes from B-site atom (Mn or Fe).

$BiFeO_3$ is one of the most extensively studied multiferroic material in recent years and it is the only material known to exhibit magnetic order (TN= 643 K) and ferroelectric order (ferroelectric transition temperature Tc FE= 1103 K) at room temperature. The properties of the material are discussed in this section [26].

2.3.1 History of $BiFeO_3$

The basic idea that crystals could be simultaneously ferromagnetic and ferroelectric probably originated with Pierre Curie in the 19th century [20]. After switching was discovered in ferroelectric Rochelle Salt by Valasek in 1920 [21] there was a rash of supposed discoveries of magnetoelectric properties by Perrier, but unfortunately in materials such as Ni in which they

are now understood to be impossible. A history of this period of solid-state physics is given in O' Dell's text [22].

True magnetoelectricity–defined as a linear term in the free energy was first understood theoretically by Dzyaloshinskii [23] with special predictions being made for Cr2O3 and discovered experimentally in that material by Astrov [24]. However, this material is paraelectric and antiferromagnetic, making microelectronics applications impractical.

The more interesting case of ferromagnetic ferroelectrics waited for some years until the work of Schmid on boracites [25]. The boracites are also impractical materials for device applications: they have low symmetry with large unit cells and grow in needle shapes; more importantly, they exhibit magnetoelectricity only at extremely low temperatures. Meanwhile Smolenskii's group in Leningrad pioneered [26] the study of bismuth ferrite, BiFeO3, but they found that they could not grow single crystals and that ceramic specimens were too highly conducting (probably caused by oxygen vacancies and mixed Fe valences) to be used in applications. They tried to address the conductivity problem by doping other ions into both the A and B sites of the lattice.

2.3.2 Crystal structure of $BiFeO_3$

The room-temperature phase of BiFeO3 is classed as rhombohedral (space group R3c) [27]. The perovskite-type unit cell has a lattice parameter, α_{pc} of 3.965A° and a rhombohedral angle, α_{pc}, of 89.3–89° at room temperature [28] with ferroelectric polarization along [111] pseudo cubic [29].

A very important structural parameter is the rotation angle of the oxygen octahedra. This angle would be 0° for a cubic perovskite with perfectly matched ionic sizes. A measure of how well the ions fit into a perovskite unit cell is the ratio (rBi + rO)/l, where r is the ionic radius of the respective ion and l is the length of the octahedral edge. This is completely analogous to the commonly used Goldschmid tolerance factor [28], which is defined as t = (rBi + rO)/(rFe + rO). For BiFeO3 we obtain t=0.88 using the ionic radii of Shannon [30], with Bi3+ in eightfold coordination (the value for 12-fold coordination is not reported) and Fe3+ in sixfold coordination and high spin. When this ratio is smaller than one, the oxygen octahedra must

buckle in order to fit into a cell that is too small. For BiFeO3, ω is ca. 11–14° around the polar [111] axis [28]. The displacement of the A-site bismuth cation (shown in Fig. 2.5) along the [111] axis brings about a non-centrosymmetric polarization resulting in the ferroelectric property.

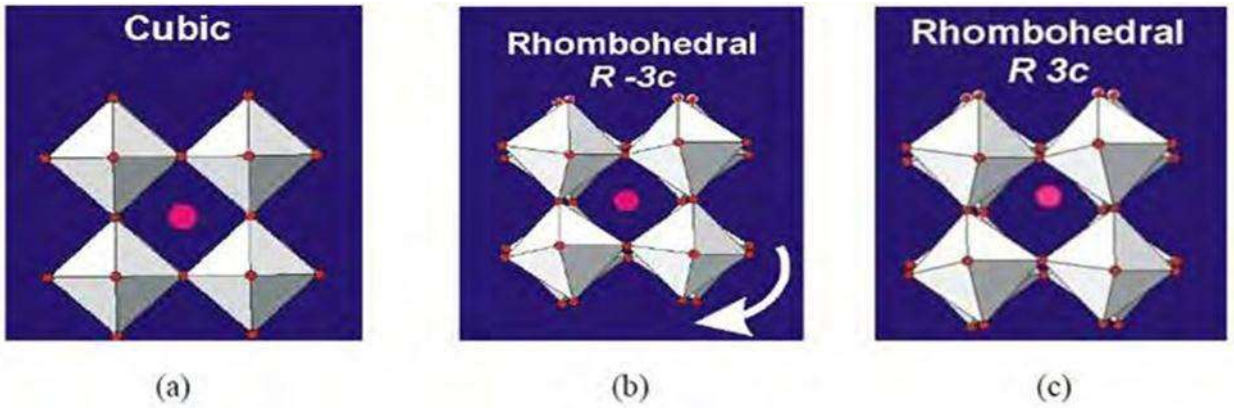


Fig. 2.5: Schematic illustration of a structural transition process (a) ideal cubic structure Pm-3m without tilting (a0a0a0); (b) R-3c structure tilted along three axes with the same angle (a-a-a-); (c) Displacement of Bi ion towards [111] direction based on R3c.

The lattice parameter and crystal structure of BiFeO3 are dependent on the temperature. It was well documented that, except for the long Bi-Fe bond distance, the lattice parameter a, c, the volume of unit cell, the short bond distance of Bi-Fe as well as the bond angles gradually increase with increase in temperature. As a consequence of these variations, magnetism and polarization are reported to be gradually reduced, and structural phase transitions are also induced from the rhombohedral distorted R3c perovskite structure to an orthorhombic Pnma structure and eventually to a cubic structure.

The unit cell can also be described in a hexagonal frame of reference, with the hexagonal c-axis parallel to the diagonals of the perovskite cube, i.e., [001] hexagonal || [111] pseudo cubic. The hexagonal lattice parameters are ahex = 5.58A° and chex = 13.90A°. The structure is shown in Fig. 2.6.

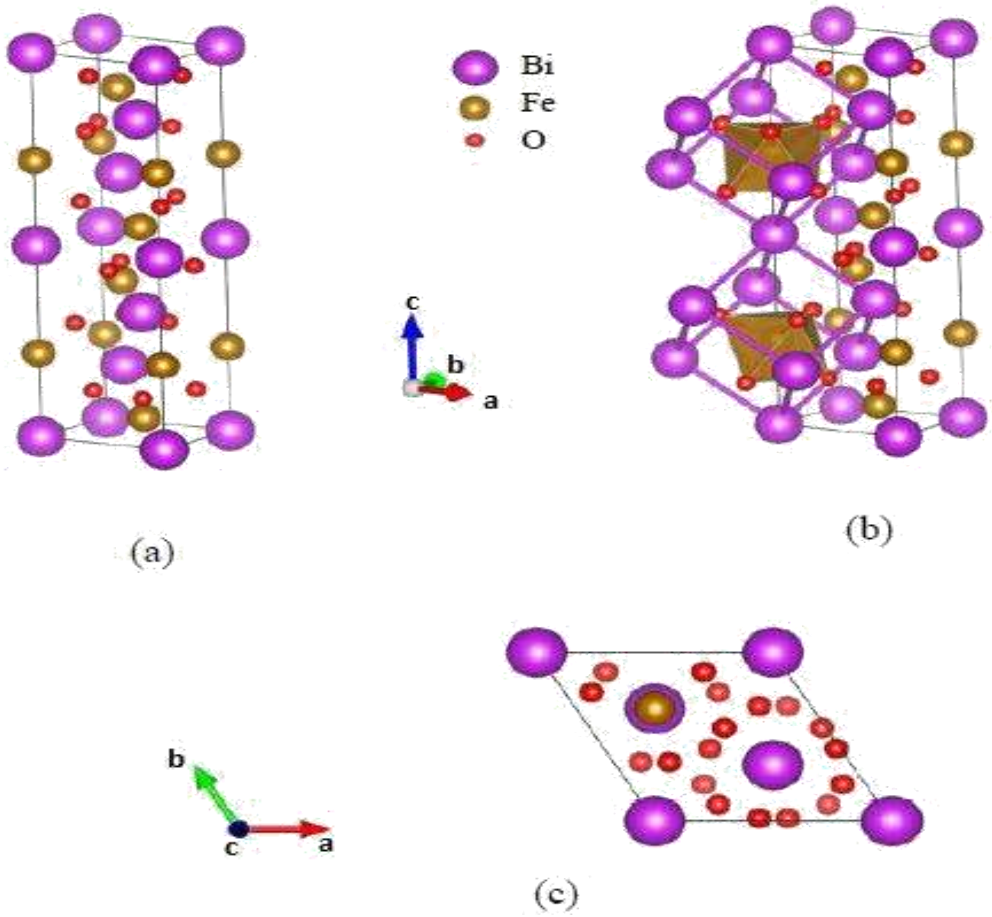


Figure 2.6: Crystal structure of bismuth ferrite (a) in the hexagonal setting, (b) in the hexagonal setting with the distorted perovskite sub-structure shown, and (c) viewed along the c-axis

In the figure, the displacement of the Bi2+ ions along the [001] direction can be easily seen. The Fe3+ ion sitting between two Bi2+ ions is not in the middle in Fig. 2.6(a). The distortion of the oxygen octahedra can also be visualized in context with the pseudo-cubic perovskite setting. The bottom octahedron is rotated along the [001] axis in relation to the top octahedron, Fig. 2.6(b). In Fig. 2.6(c) the three-fold symmetry of the structure due to the 3-fold axes running perpendicular to the page is shown.

2.3.3 Ferroelectric properties $BiFeO_3$

The ferroelectric state arises from a large displacement of the Bi ions relative to the FeO6 octahedral in BiFeO3 as shown in Fig. 2.11. The ferroelectric polarization lies along the pseudo cubic <111> leading to the formation of eight possible polarization variants, corresponding to four structural variants [31].

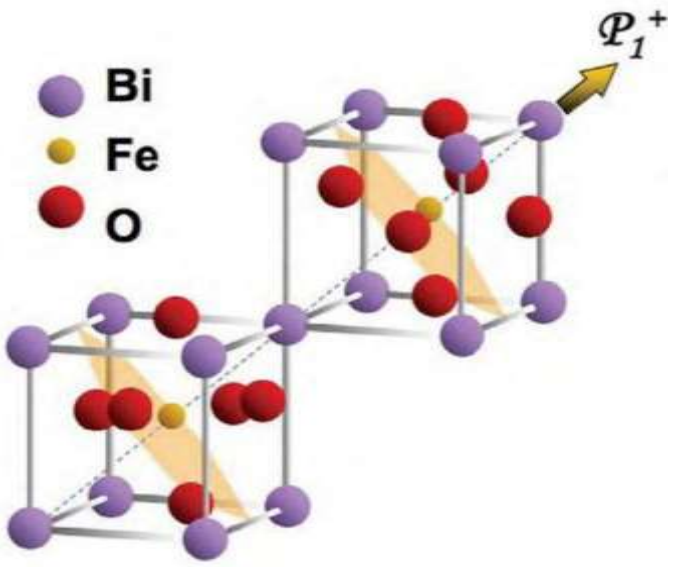


Figure 2.7: Schematic of crystal structure of BFO and ferroelectric polarization (arrow)

Electrical characterization on bulk BiFeO3 has been very difficult due to the low resistivity of samples. The controversy about whether it is ferroelectric or antiferroelectric was finally settled based on the hysteresis loop measured by Teague et al. [32]. They performed the experiment in liquid nitrogen, which lowered the charge carrier density and mobility, and in turn lowered the leakage current. The measured spontaneous polarization was 3.5μC/cm2 along the <100> direction, which represents 6.1μC/cm2 in the <111> direction. This value is much smaller than what would be expected for a ferroelectric material with such high Curie temperature and large distortion. The leakage problem, likely due to defects and non-stoichiometry, has been hampering more comprehensive studies about the bulk BiFeO3 and has limited applications of

this material. To overcome this problem, recent work has focused on reducing leakage current using proper dopants or other methods.

2.3.4 Magnetic order of $BiFeO_3$

The local short range magnetic ordering of BFO is G-type antiferromagnetic: each Fe3+ spin is surround by six antiparallel spins on the nearest Fe neighbors (Fig. 2.8). The anti-parallel alignment is a result of the super-exchange (or Kramer–Anderson super exchange) interaction [33], which is the strong (usually) antiferromagnetic coupling between two next-to-nearest neighbor cations through a non-magnetic anion. In this way, it differs from direct exchange in which there is coupling between nearest neighbor cations not involving an intermediary anion.

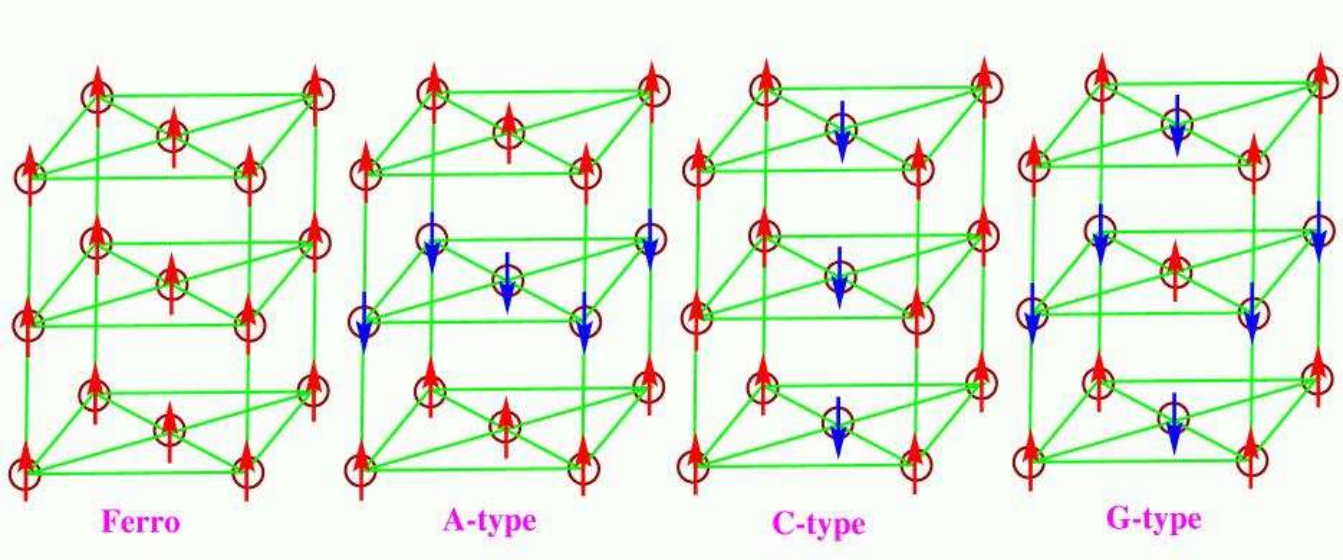


Figure 2.8: Schematic showing different types of magnetic ordering – the last three are types of antiferromagnetism

Unlike a perfect antiferromagnet, however, the spins are not exactly anti-parallel to each other. There is a small canting angle, a slight tilt in each of the spins away from perfect co-linearity. Spin canting is due to two factors contrasting each other: isotropic exchange would align the spins exactly anti-parallel, while antisymmetric exchange arising from relativistic effects (spin-

orbit coupling) would align the spins at 90° to each other [34]. The net result, as shown in Fig. 2.9, is a small perturbation, the extent of which depends on the relative strength of these effects.

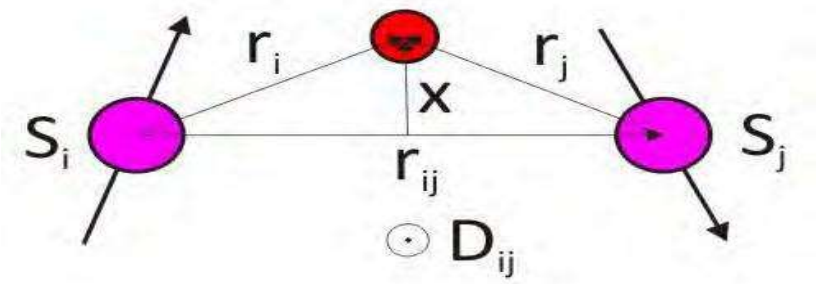


Figure 2.9: Spin canting due to anti-symmetric exchange

On top of the canted anti-ferromagnetic ordering there is a spatial modulation of the spins. The spin ordering is not homogeneous but is superimposed by an incommensurate cycloid structure with a wavelength of ~ 64 nm along <10-1>pseudo-cubic, as is shown in Fig. 2.14 [37]. The spin rotation plane can also be determined because the magnetic scattering amplitude, in case of neutron diffraction, depends on the component of magnetic moments perpendicular to the scattering vector [35]. The magnetic Néel temperature is about 643 K and the cycloid could be distorted at low temperatures [36].

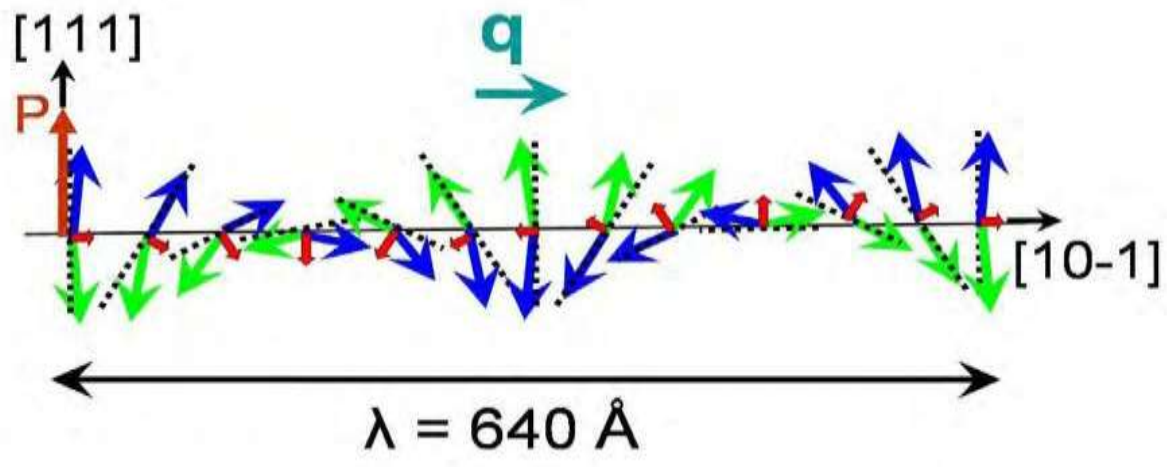


Figure 2.10: Schematics of the 64 nm antiferromagnetic circular cycloid. [The canted antiferromagnetic spins (blue and green arrows) give rise to a net magnetic moment (purple arrows) that is specially averaged out to zero due to the cycloidal rotation. The spins are contained within the plane defined by the polarization vector [50].

So far, various origins have been proposed, such as the bulk photovoltaic effect [38], depolarization field driven photovoltaic effect [39], Schottky barriers [40], and domain wall theory [41]. However, there are still a lot of disputes and controversy on the photovoltaic origins and they deserve further studies undoubtedly.

2.3.5 Synthesis and Phase Diagram of $BiFeO_3$

$BiFeO_3$ is a typical multiferroic material that has been extensively investigated nowadays. The initial research on $BiFeO_3$ was carried out by Smolenskii in1960 [42]. But at that time, they were not able to make single-phase polycrystalline$BiFeO_3$ and the BiFeO3 produced was not stable for practical application. In 1967, Achenbach successfully prepared single-phase $BiFeO_3$ by removing the undesirable phases using HNO_3 [30]. X-ray diffraction technique was also adopted to investigate the mono domain single-phase by Kubel and Schmid in 1990. Later in 2003, Ramesh and his colleagues produced thin film $BiFeO_3$ which exhibited remnant polarization 15 times stronger than that of the bulk $BiFeO_3$. Until recently, increasing effort have also been devoted to the research focusing on the preparation and characterization of $BiFeO_3$ in forms of film, bulk and nanostructure.

However, single phase $BiFeO_3$ is difficult to synthesize. Due to the metastable nature of bismuth ferrite in air 20 as well as the volatility of bismuth oxide, their stoichiometry can be changed resulting in impurities of Bi_2O_3, $Bi_{25}FeO_{39}$ and Bi_2FeO_9 during the sintering process. The phase diagram of Fe_2O_3 and Bi_2O_3 is presented below in Figure 2.16, unequal amount of Fe_2O_3 and Bi_2O_3 is seen to bring about impurity phases $Bi_{25}FeO_{39}$ (bismuth-rich) and Bi_2FeO_9 (bismuth- deficient)

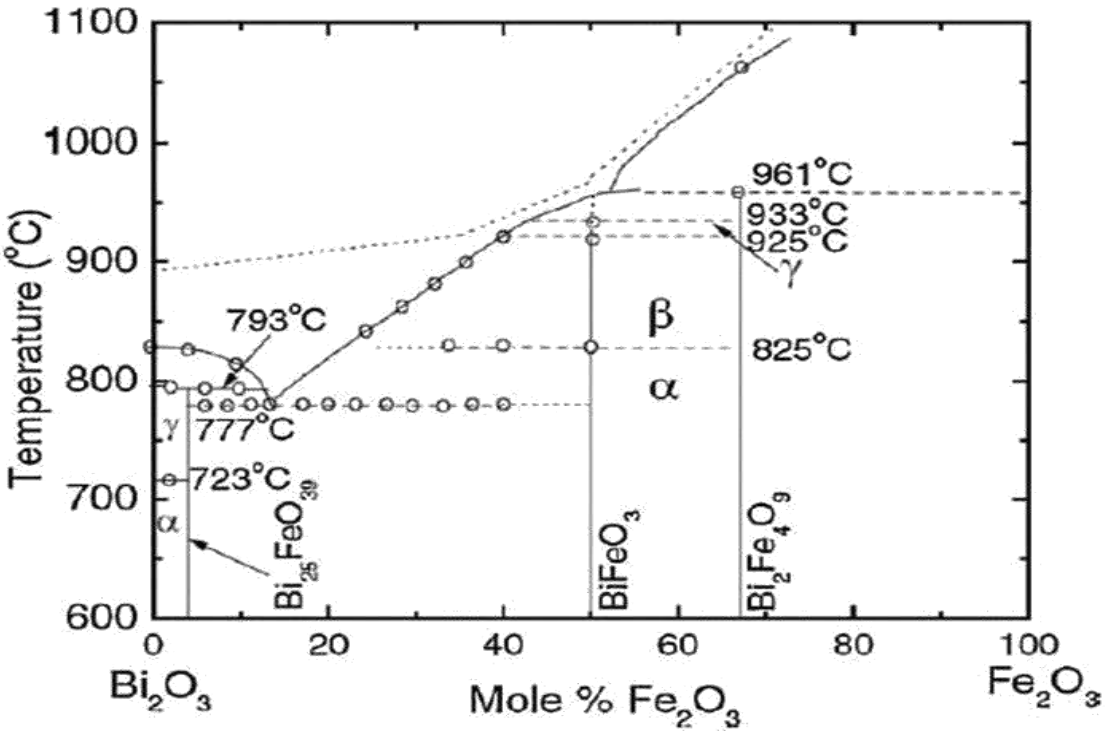


Figure 2.11: Phase diagram of $Fe_2O_3$and Bi_2O_3showing bismuth ferrite with undesired impurities [43].

CHAPTER 3

EXPERIMENT

3.1 Introduction

Among the various wet chemical processes, the pechini sol-gel route is found to be simple and cost effective for the synthesis of homogeneous and very fine crystalline nano powders. The process is based on the mixing of reactants that oxidize easily, such as metal nitrates, and an organic chelating agent that acts as reducing agent. The various advantages of sol-gel synthesis as the prime method for the production of BiFeO3 are

- Self-purification due to the high exothermic temperatures involvement.
- Formation of Nano- powders in the desired size and shape with uniform particle size distribution.
- Simple and cost-effective.
- Synthesis of single phase materials at very low temperatures.

3.2 Synthesis Procedure

Bismuth ferrite was prepared by a modified pechini sol-gel method using Citric acid as the chelating agent. The reagents used in the present work were analytical grade bismuth nitrate pentahydrate (Bi(NO3)3·5H2O), iron nitrate monohydrate (Fe(NO3)3·9H2O), citric acid (C6H8O7), ethylene glycol (C2H6O2) and glacial acetic acid (CH3COOH). Procedure steps are as follow:

1. Stoichiometric proportion of $Bi(NO3)_3.5H2O$ and $Fe(NO_3)_3.9H2O$ were initially dissolved in 400 ml deionized water with an individual concentration of 0.025M.
2. The solution was stirred for about half an hour to obtain a clear solution.
3. When the solution was transparent, 0.02 mole of $C_6H_8O_7$ as the chelating agent was

added to the solution to complex the metal cations (Figure 3.1a).

4. The solution was then stirred and heated at 70-75°C for 8-10 hrs. to form a transparent blackish-red sol (Figure 3.1b).
5. pH of the solution was maintained between 1-2 all-time by adding NH_4OH dropwise.
6. Afterwards appropriate amount of ethylene glycol was added to the solution as polymerization agent.
7. The resultant solution was heated at 85-90°C to initiate the polymerization reaction and a few minutes later a gel was formed with vigorous boiling and fuming (Figure 3.1c).
8. The gel was dried at 100°C for 24 hrs. in a drier to obtain fluffy green xerogel (Figure 3.1d).
9. The same procedure was repeated to produce xerogel for annealing at different temperatures.
10. The xerogel samples were then grounded into powders and annealed at 700°C for 2 hrs. in static air to get BiFeO3 nanoparticles
11. Another xerogel sample was also annealed at temperature as high at 800°C to obtain bulk BiFeO3 sample.
12. The heating and cooling rate of the furnace were maintained at 3°C/min.
13. The powders thus obtained were washed with CH_3COOH followed by deionized water at 70 °C to remove impurity phases from $BiFeO_3$.
14. Finally, the powders were dried for characterization.

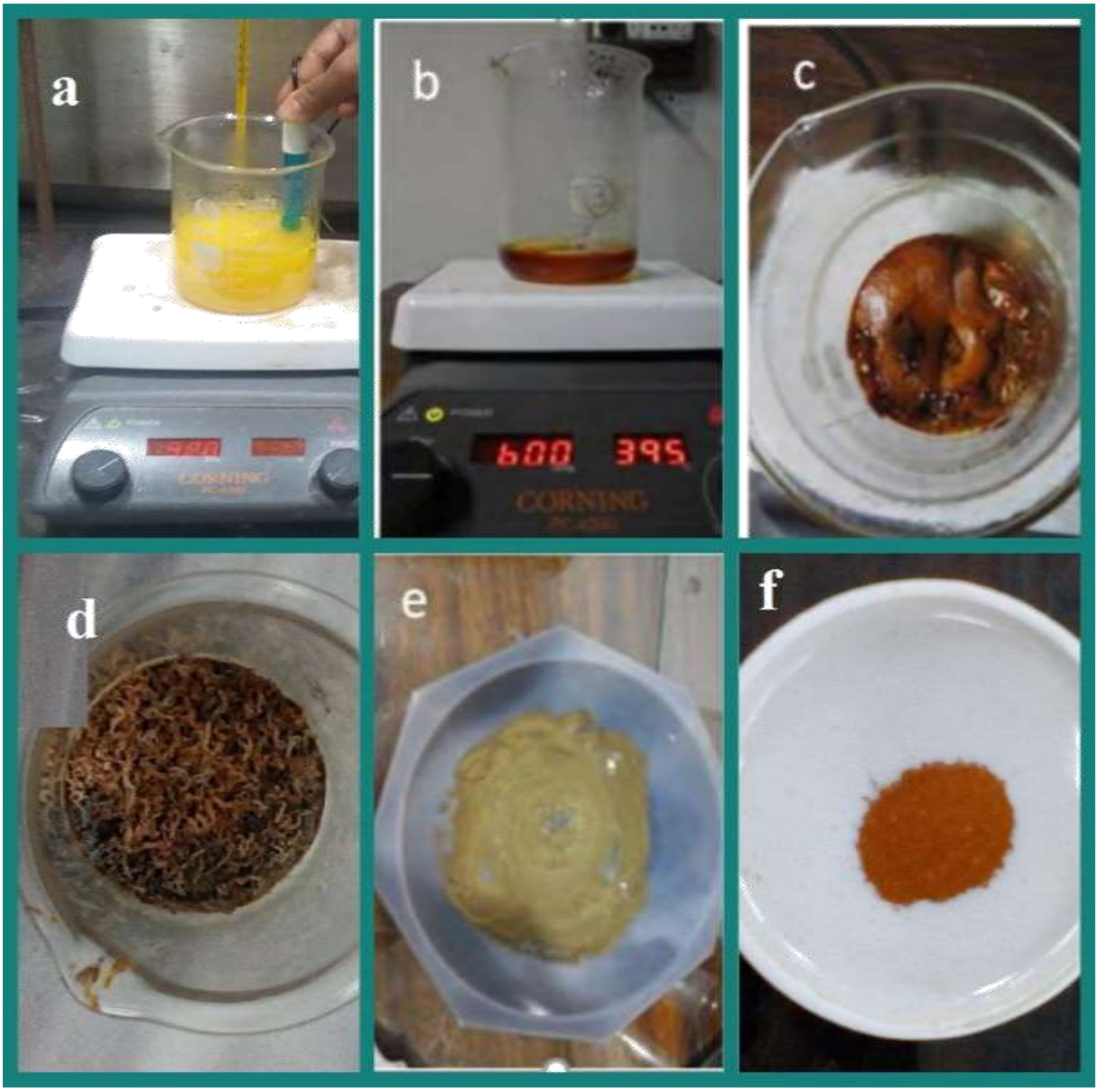


Figure 3.1: Synthesis steps a) mixing raw materials into deionized water, b) formation of sol, c) formation of gel, d) precursor xerogel e) ground xerogel, f) annealed $BiFeO_3$ powder

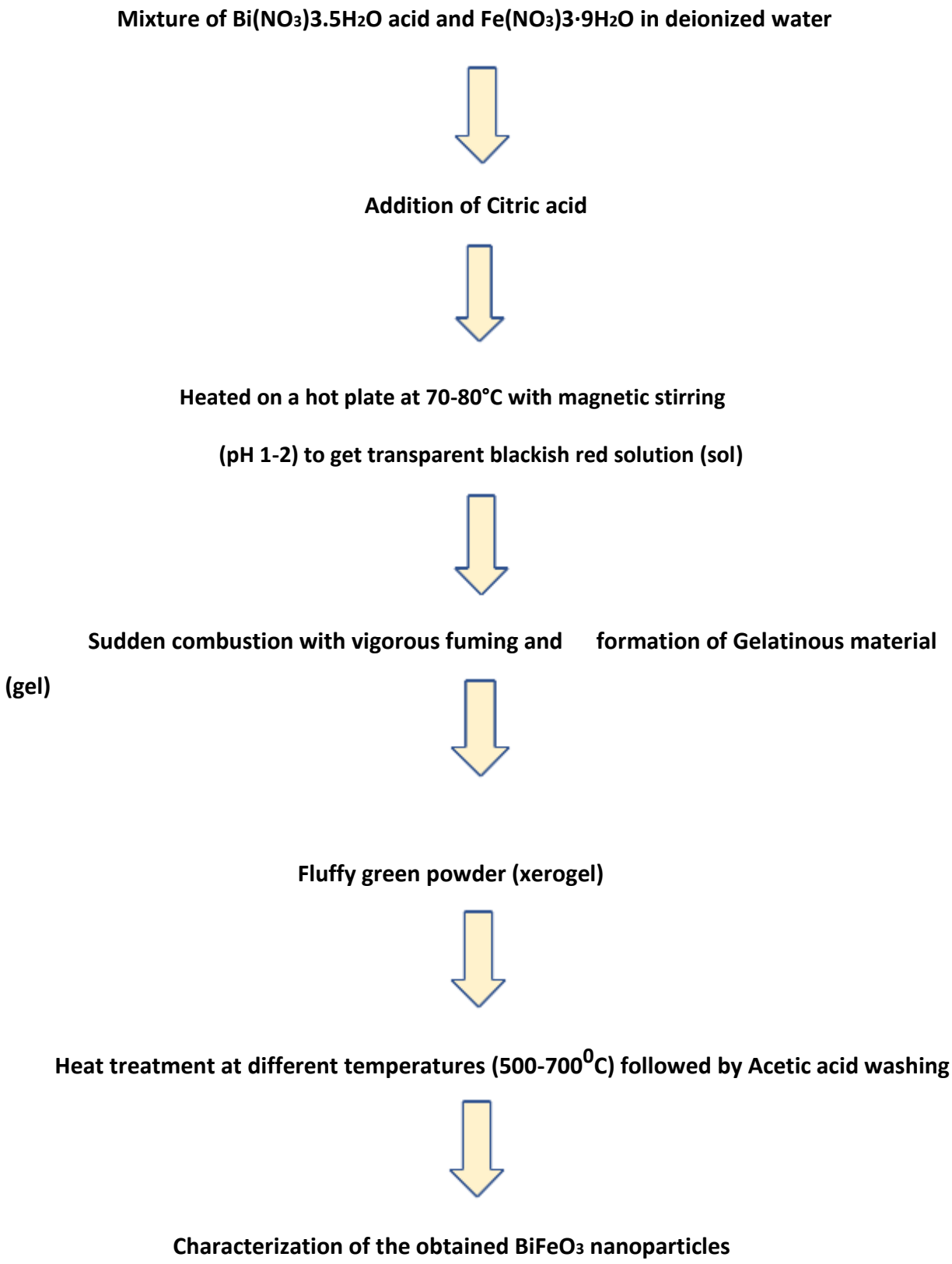


Figure3.2: Flow chart for $BiFeO_3$ powder synthesis

3.3 Annealing

Muffle Furnace (NaberthermGmbltBahnhofstr, 20, Lilienthal / Bremen Germany) was used to anneal xerogel samples at 700°C in air atmosphere. The basic annealing cycle in this experiment is shown in Figure 3.3.



Figure 3.3: Furnace used for annealing xerogel

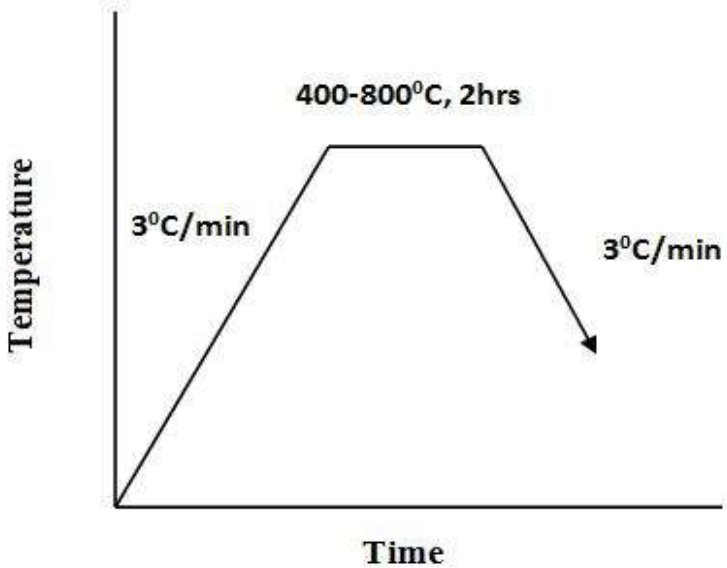


Figure 3.4: Annealing cycle

3.4 Muffle Furnace

A muffle furnace or muffle oven (sometimes retort furnace in historical usage) is a furnace in which the subject material is isolated from the fuel and all of the products of combustion, including gases and flying ash. After the development of high-temperature heating elements and widespread electrification in developed countries, new muffle furnaces quickly moved to electric designs.

Historically, small muffle ovens were often used for a second firing of porcelain at a relatively low temperature to fix overglaze enamels; these tend to be called muffle kilns. The pigments for most enamel colors discolored at the high temperatures required for the body and glaze of the porcelain. They were used for painted enamels on metal for the same reason.

Today, a muffle furnace is (usually) a front-loading box-type oven or kiln for high-temperature applications such as fusing glass, creating enamel coatings, ceramics and soldering and brazing articles. In ceramics muffle kilns were typically used for relatively low temperatures, for overglaze decoration. They are also used in many research facilities, for example by chemists in order to determine what proportion of a sample is non-combustible and non-volatile (i.e., ash). Some digital controllers allow RS232 interface and permit the operator to program up to 126 segments, such as ramping, soaking, sintering, and more. Also, advances in materials for heating elements, such as molybdenum disilicide, can now produce working temperatures up to 1,800 degrees Celsius (3,272 degrees Fahrenheit), which facilitate more sophisticated metallurgical applications.

The term muffle furnace may also be used to describe another oven constructed on many of the same principles as the box-type kiln mentioned above, but takes the form of a long, wide, and thin hollow tube used in roll-to-roll processes.

Both of the above-mentioned furnaces are usually heated to desired temperatures by conduction, convection, or blackbody radiation from electrical resistance heater elements. Therefore, there is (usually) no combustion involved in the temperature control of the system, which allows for much greater control of temperature uniformity and assures isolation of the material being heated from the byproducts of fuel combustion.

3.5 Field Emission Scanning Electron Microscopy

To observe morphology of the synthesized powders we used field emission scanning electron microscope, FESEM (JEOL JSM 7600F). Powder samples were adhered with carbon tape that was attached to a Copper stub. Samples were made conductive, coated with platinum by ion sputtering method. Then sample holder was mounted on a holder and inserted in FESEM. The micrographs obtained from FESEM analysis was used for microstructural study.



Figure 3.5: Field Emission Scanning Electron Microscope (FESEM).

3.6 X-Ray Diffraction Study

X-rays are a type of electromagnetic radiation. The wavelength of x-rays is approximately 1 Å which has the same size equivalent to that of an atom. X-ray diffraction (XRD) is a non- destructive analytical technique mainly used for the phase identification and structural characterization of crystalline materials.

X-ray diffraction analysis was conducted using the XRD (3040-X‟Pert PRO, Philips) facility in order to determine the phases present in the synthesized powers. The high-intensity CuKα

radiation was focused on the sample in the scanning range from 10° to 70°.



Figure 3.6: XRD Machine

The relationship between the wavelengths of the X-rays λ, the incidence angle θ, and spacing between two crystal lattice planes (hkl) d, is shown in the Bragg's Law expressed as:

= .....( )

After characterization by X-ray diffraction, a number of peaks are seen in the diffraction patterns. These patterns are identified by comparing their positions and relative intensities with the known structures in the database. Sometimes extra peaks might appear due to the impurity or structural transformation after thermal treatment. In fact, the intensity, width and position of peaks in the patterns reflect information about structure, quantity, texture etc. of crystallites.

The average crystallite size (d) of the synthesized powders was calculated from the XRD patterns using the Scherrer formula,

$$= \quad / \qquad \ldots\ldots\ldots\ldots\ldots\ldots\ldots\ldots\ldots\ldots ( )$$

where k is the dimensionless shape factor with a typical value of about 0.9, λ is the wavelength of Cu Kα radiation with the value of 1.5418 Å, θ is the Bragg angle for the diffraction peak and β is the full width at half maximum intensity (FWHM) of the corresponding diffraction peak.

3.7 UV Spectra Study

Ultraviolet Visible Spectrophotometry (UV–Vis or UV/Vis) refers to absorption spectroscopy or reflectance spectroscopy in part of the ultraviolet and the full, adjacent visible spectral regions. This means it uses light in the visible and adjacent ranges.

The optical Eg of BFO nanoparticles was measured by the diffuse reflectance spectra using a UV–Vis–NIR spectrophotometer (Model: PerkinElmer UV–Vis–NIR Spectrometer Lambda 1050) shown in the figure 3.8.



Figure 3.7: PerkinElmer UV–Vis–NIR Spectrometer Lambda 1050

3.8 PL Spectra Study

Photoluminescence spectroscopy, often referred to as PL, is when light energy, or photons, stimulate the emission of a photon from any matter. It is a non-contact, nondestructive method of probing materials. In essence, light is directed onto a sample, where it is absorbed and where a process called photo-excitation can occur. The photo-excitation causes the material to jump to a higher electronic state, and will then release energy, (photons) as it relaxes and returns to back to a lower energy level. The emission of light or luminescence through this process is photoluminescence, PL.

The optical Eg of BFO nanoparticles was measured by the PL spectra using a Microscope Optical Spectrometer (Model: FLS – 1000) shown in the figure 3.9.



Figure 3.8: PL spectra Machine FLS - 1000

CHAPTER 4

RESULTS AND DISCUSSION

4.1 Introduction

At the very beginning conventional Pechini Sol-Gel route was adopted to synthesize nanoparticles using citric acid as a chelating agent. The advantages of using citric acid include low decomposition temperature and synthesis of materials with homogeneous microstructure. Synthesis of pure and very uniformly distributed particles is really difficult. In the present work, a systematic study is reported on the effect of particle size on structural and bandgap properties of BiFeO3 nanoparticles.

.

4.2 X-ray diffraction (XRD)

The nanoparticles were characterized by X-ray diffraction(XRD) (model: PANAlALYTICAL EMPYREAN) at room temperature. The high intensity X-ray beams were diffracted on the samples for the scanning limit from 10–70◦. Figure shows the XRD patterns for BFO nanoparticles at 700°C. XRD patterns of particles annealed at 700°C before and after washing with CH_3COOH. To promote the formation of $BiFeO_3$, the samples were heat treated at 700°C for 2 hrs. Usually a strong acid (HNO_3) is used to remove the secondary phases that are formed during synthesis of $BiFeO_3$ nanoparticles. But HNO_3 may dissolve the $BiFeO_3$ phase [38]. So CH_3COOH, a week acid was used for washing purpose in this research. XRD patterns clearly confirmed the crystalline nanoparticles from the synthesized samples. Generally, mullite $Bi_2Fe_4O_9$ is frequently reported secondary phases that are formed during synthesis of BFO. The secondary phase in BFO is the main concern because Bi^{3+} and/or Fe^{3+} vacancies assist in creating these types of secondary phases. The low temperature stability of impurity phases, metastable and off-stoichiometric nature of $BiFeO_3$ are thought to be the prime causes for the formation of secondary phases [45- 47]. However, removal of these phases is important from

the application point of view because they increase leakage current and deteriorate ferroelectric property [44]

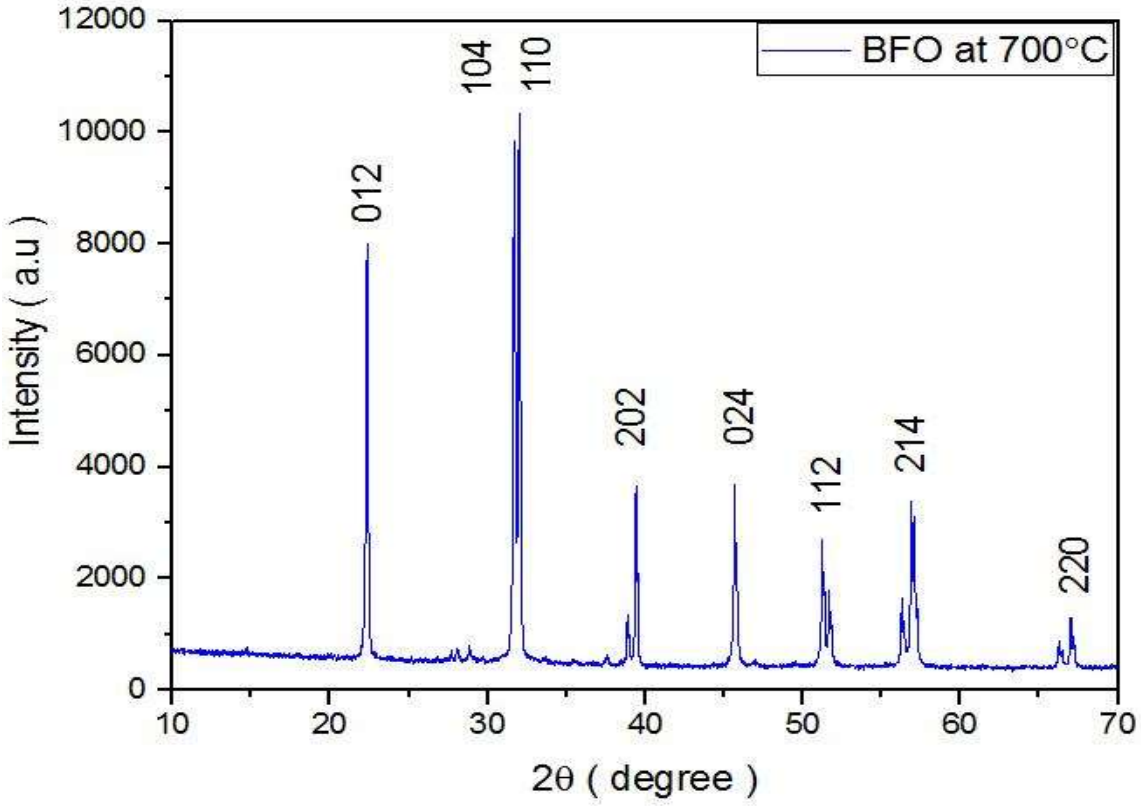
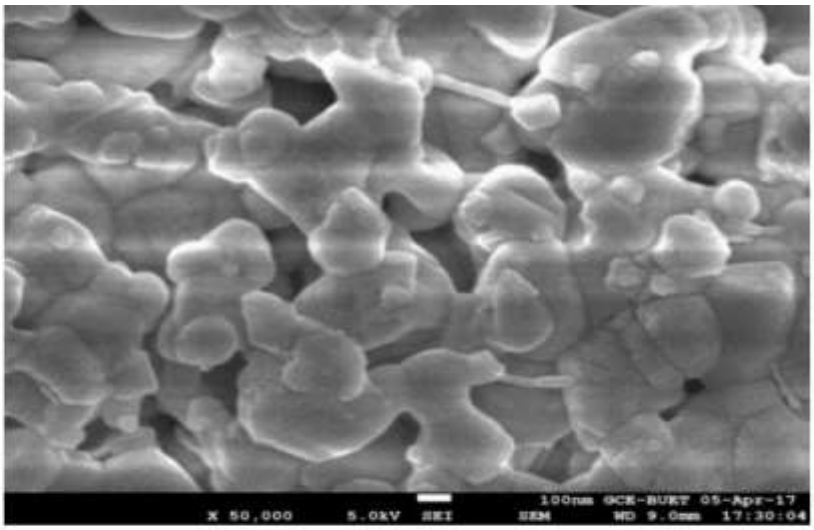


Figure 4.1: X-ray diffraction patterns of BiFeO3 particles annealed at different temperatures (a) after washing with acetic acid. (b) Magnified XRD patterns of (102) reflection plane and (c) magnified XRD patterns of (104) and (110)

4.3 FESEM micrograph analysis

Figure shows the FESEM micrographs of BiFeO3 powders annealed at temperature range 700°C for 2 hrs. Reduction of the total surface area by an increase in the average size of the particles is the driving force behind coarsening. At high temperature vapor pressure is high on smaller particles than coarser particles. So small particles vaporize and condense on larger particles. In this mechanism attainment of uniform particle size distribution is difficult. It is evident from the figure that the particle sizes observed from FESEM micrograph are quite compatible with that of XRD results. This suggests that the nanoparticles are single

crystalline. BiFeO3 sample annealed at 700°C showed stable cubic morphology. The particle size measured from the FESEM micrographs with the help of “imageJ” software and it was 212 nm.



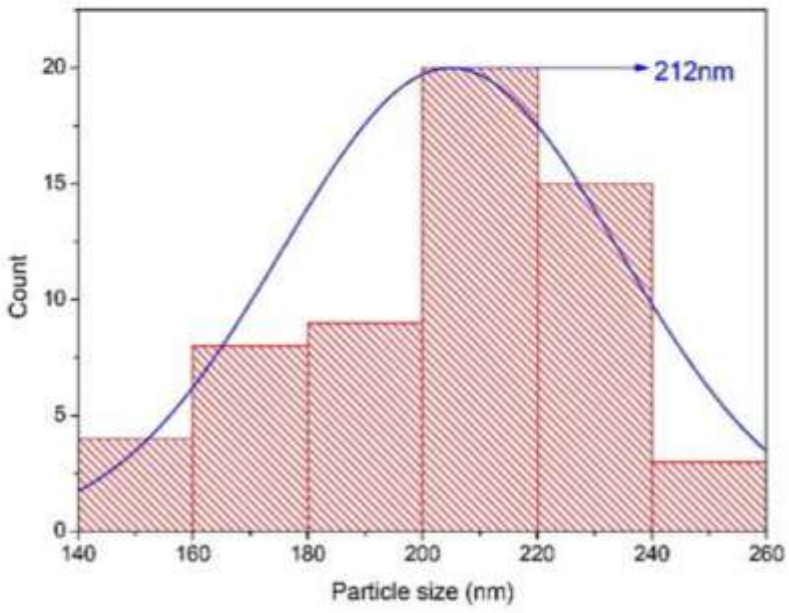


Figure 4.2: FESEM micrographs with particle size at 700°C

4.4 EDS Data Analysis of the BiFeO3 nano Particle

EDS has confirmed the composition of the products. Figure 7 shows the EDS spectra of BiFeO3 particles. The EDS spectrum pointed out the presence of bismuth, iron, and oxygen of the prepared sample. The composition of the elements in the sample obtained by the Sol-gel method was 67.21%; 16.36%; and 15.74% for bismuth; iron and oxygen, respectively. Figure 4.3 shows EDS data analysis of the BFO powder.

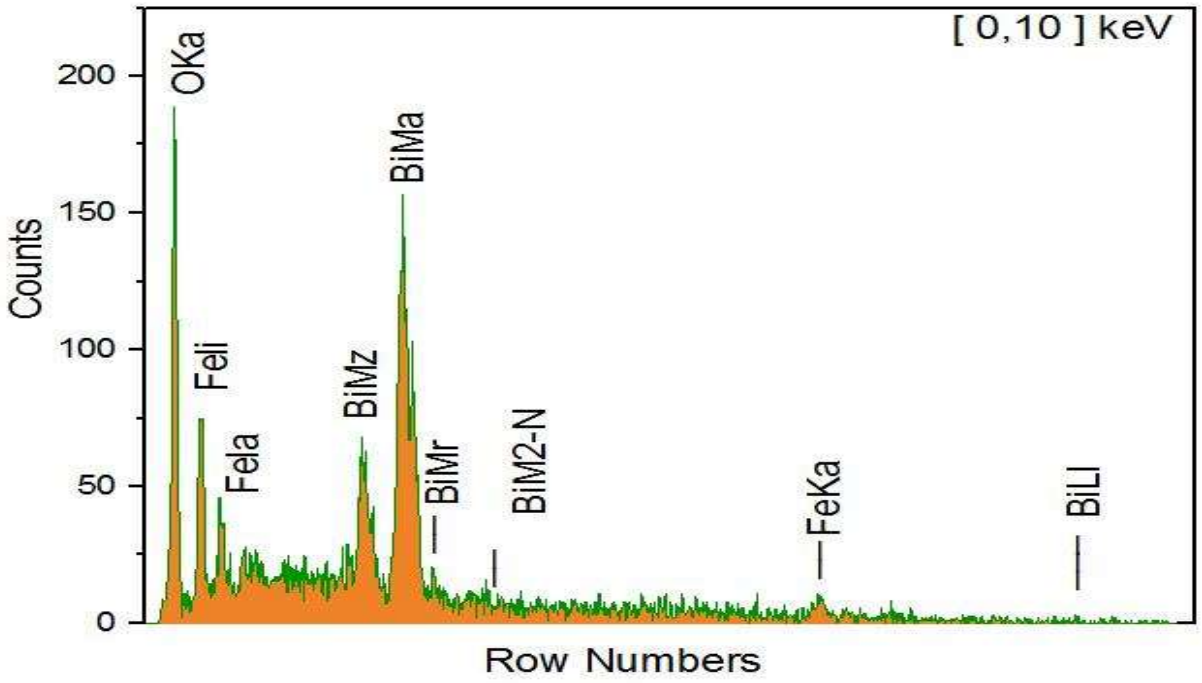


Figure-4.3: EDS patterns of BFO nanoparticles.

4.5 Bandgap Engineering

Because of small band gap energy, BFO is very effective as a visible-light irradiator. It is established that the PV absorption ability of BFO is directly related to its electronic structure and is considered as the key factor to calculate its band gap energy [18]. The optical Eg of BFO nanoparticles was calculated by the two different methods. Those are as follow:

- UV Spectroscopy

- PL Spectroscopy

4.5.1 UV Spectrometry

Figure 4.4 presents the $[F(R)hv]^2$ vs. eV (bandgap energy, eV) plots for all nanoparticles. Basically, solar radiation with wavelengths ranging from 380 to 750 nm (violet to red) strikes the material with enough energy to knock electrons from their weak bonds and create an electric current. The unused wavelengths, ultraviolet (10–380 nm) and infrared (750– 1,000,000 nm) do not have enough energy to dislodge the electrons and are absorbed as heat. Thus, we considered the wavelength range of 200–800nm for capturing the data. The intersection of the tangent line at $[F(R)hv]^2 = 0$, indicates the bandgap energy, eV [19], which is correlated with the energy (eV) difference between the valence band (VB) (O 2p) and the conduction band (CB Fe 3d) of BFO. The obtained value of the bandgap Eg for pure BFO at 700°C from the figure is 1.92 eV.

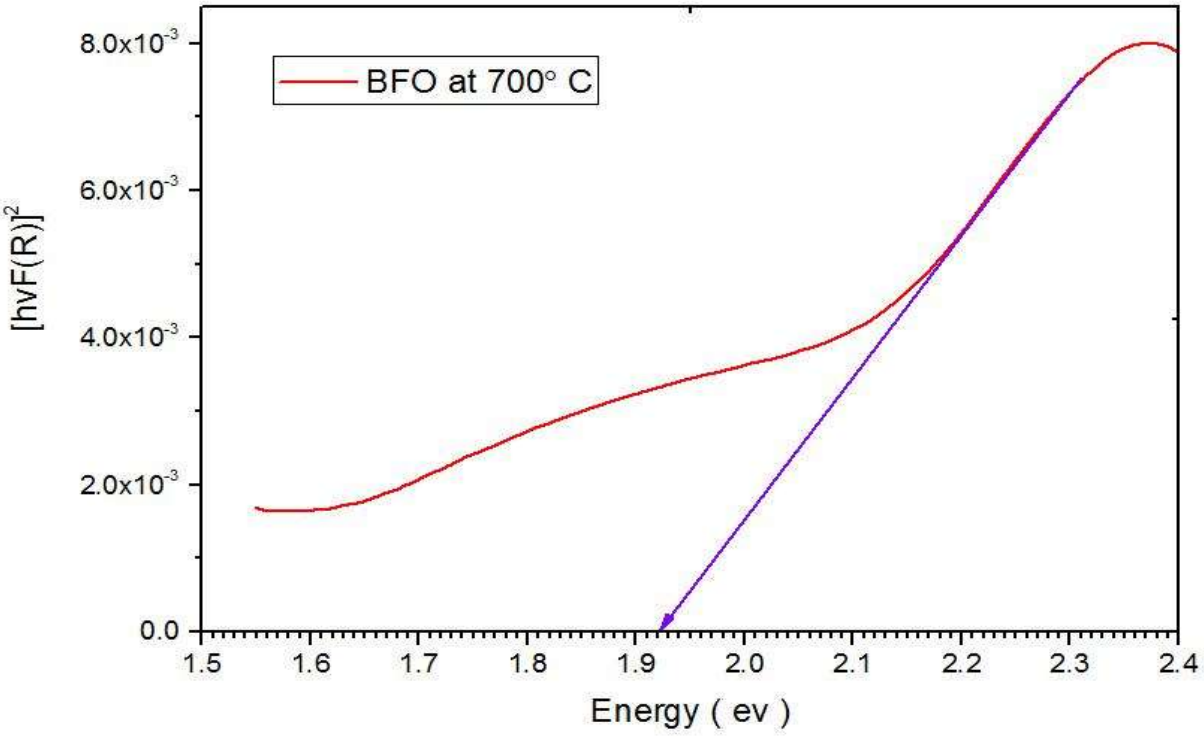


Figure 4.4: $[F(R)hv]^2$ Vs eV for pure Bismuth ferrite at 700°C

4.5.2 PL Spectrometry

In order to examine the PL properties of pure BFO nanoparticles, the PL spectra were recorded in the range of 200–900 nm at an excited wavelength of 200 nm at room temperature, as shown in Figure 4.5

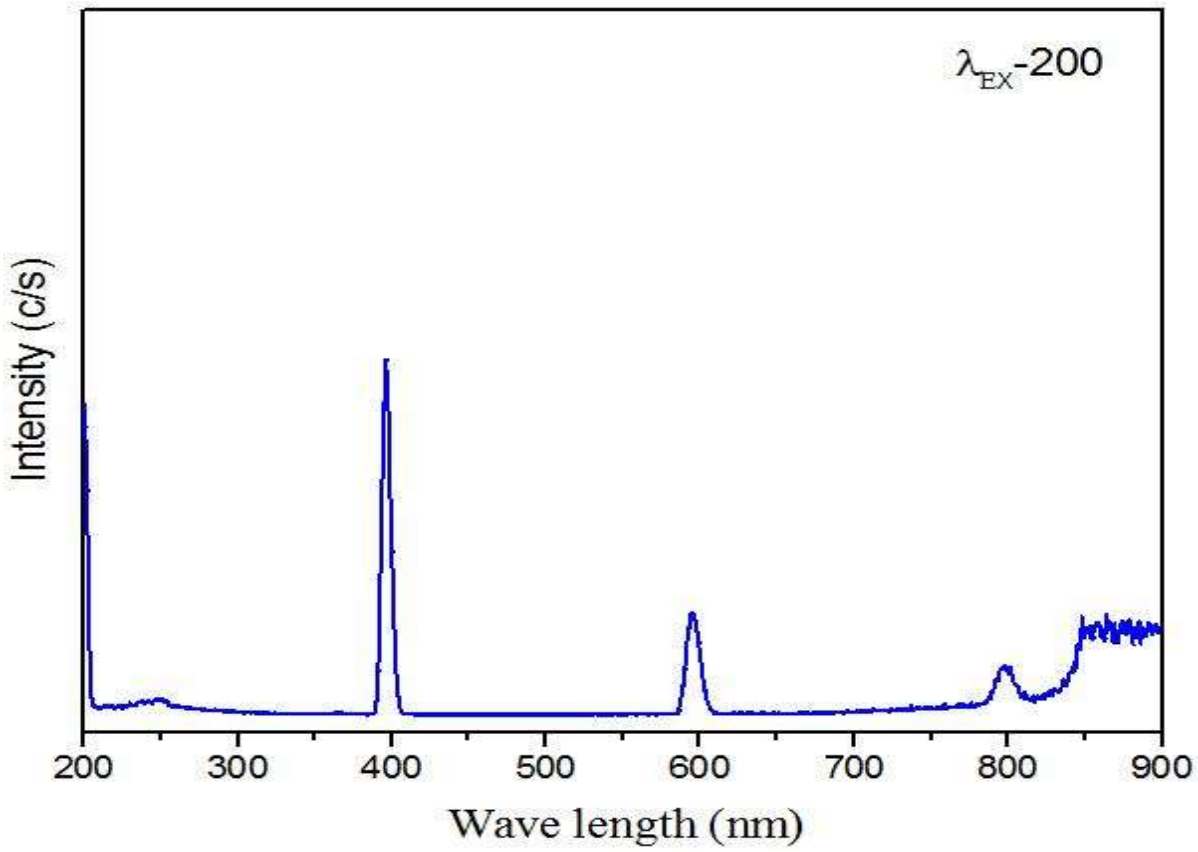


Figure 4.5: Intensity Vs eV for pure Bismuth ferrite at 700°C

After deconvolution three peaks could be identified at 400 nm, 600 nm and 800 nm. The strong blue emission peak at the wavelength of 400 nm may arise from self-activated centers in the synthesized nanoparticles. In principle, pure BFO only has the intrinsic emission arising from the band-to-band transitions. Any other emission of longer wavelengths came from various

defect and/or impurity levels inside the bandgap. So, only peak that is to be considered here is at 600 nm.

Following equation is used to calculate the bandgap:

$$= (\quad)/ \quad \ldots\ldots\ldots\ldots\ldots\ldots\ldots\ldots\ldots\ldots \textbf{(7)}$$

Here,

E = Bandgap Energy

h = Planck's constant = $6.62607004 \times 10^{-34}$ m^2 kg / s

c = Velocity of Light in Vacuum = 3×10^8 m/s

λ = Wavelength of the actual peak from the figure x = 600 nm

Putting all the values in the equation (10), bandgap of Eg for pure BFO was calculated 2.06 eV which is very near to the bandgap measured from UV spectrometry.

Table 4.1: Particle size and bandgap of $BiFeO_3$ by UV & PL Spectroscopy

BFO Annealing Temperature (°C)	**Particle size (nm)**	**Bandgap (eV) by UV Spectroscopy**	**Bandgap (eV) by PL Spectroscopy**
700	212	1.92	2.06

CONCLUSION

The objective of this thesis project was to produce good quality BFO thin films using cost effective raw materials and simple sol-gel processing route and to analyze the properties multiferroic material $BiFeO_3$ including bandgap measurement. To minimize the costs, we have used metal nitrates instead of the more expensive metal alkoxides and have employed citric acid instead of acetic anhydride as chelating agent. Although some limitations were faced, we believe our goal has been largely achieved in that we have managed to tune the processing parameters and fabricate dense, well crystallized films with very good phase purity. Our findings can be summarized as follows:

I. BiFeO3 nanoparticles were synthesized via a soft chemical route. Nearly pure and well crystallized BiFeO3 powders were obtained by washing with acetic acid instead of conventional nitric acid.

II. Ethylene glycol with an optimum concentration of 0.05 M was successfully used as surfactant agent during synthesis to obtain a homogenous and uniform particle size distribution.

III. BFO had been annealed at 700^0 C.

IV. FSEM Micrograph, X-Ray Diffraction, EDS Data were studied to find out the properties of $BiFeO_3$.

V. The sizes of the synthesized BiFeO3 nanostructures calculated by ImageJ software from the FSEM data analysis were noted to be 212 nm.

VI. UV Spectra and PL Spectra were studied to calculate the bandgap Eg separately to confirm the of accuracy and were noted to be 1.92 eV and 2.06 eV respectively.

SUGGESTIONS FOR FUTURE WORK

- Commercialization of the synthesis technique.
- Making the seed layer discontinuous by keeping the preheat temperature low, could also help in creating films that are more textured.
- Inducing higher degrees of texture should be attempted. Making a thinner seed layer and depositing a greater number of subsequent layers on top should bring about better columnar grain structure and texture.
- Synthesis of BiFeO3 nanoparticles using different chelating agent and surfactant.
- Synthesis of doped (Ba, Mn, La, Gd, Nd, Nb, Dy etc) $BiFeO_3$ nanoparticles.
- Fabrication of thin film to reproduce high magnetization in this structure.

Reference

[1]. REN21 (2017). "Renewables global futures report 2017"

[2]. Geo-Heat Centre Quarterly Bulletin, Klamath Falls, Oregon: Oregon Institute of

[3]. Schmidt-Rohr, K. "Why Combustions Are Always Exothermic, Yielding About 418 kJ per Mole of O2", J. Chem. Educ. 92: 2094-2099,2015.

[4]. H. Ibach, H. Luth, “Solid-State Physics: An Introduction to Principles of Materials Science”, 4th edition, Springer Dordrecht Heildberg, London New York, 2009.

[5]. Principles of Electronic Materials - S.O. Kasap.

[6]. http://www.nrel.gov/ncpv/

[7]. J. Silva, A. Reyes, H. Esparza, H. Camacho, L. Fuentes, “BiFeO3: A review on synthesis, doping and crystal structure” Integrated Ferroelectrics, Vol. 126, 2011, pp 47-59.

[8]. S. Somiya, F. Aldinger, “Handbook of Advanced Ceramics: Processing and their applications”, Vol-2, Elsevier Academic Press, 2009.

[9]. [9] W. Eerenstein, N. D. Mathur, J. F. Scott, “Multiferroic and magnetoelectric materials” Nature, Vol. 442, 2006, pp 759-765.

[10]. M. Fieberg, “Revival of the magnetoelectric effect”, Journal of Physics D: Applied Physics, Vol. 38, 2005, pp.123.

[11]. A.K. Ghosh , G.D. Dwivedi, B. Chatterjee, B. Rana, A. Barmanb, S. Chatterjee, H.D. Yang, “Role of codoping on multiferroic properties at room temperature in BiFeO3 ceramic”, Solid State Communications, Vol. 166, 2013, pp22–26.

[12]. Nicola A. Hill, “Why are there so few magnetic ferroelectrics?”, Journal of Physical Chemistry B, Vol. 104, 2000, pp6694-6709.

[13]. T. Kimura, “Magnetic control of ferroelectric polarization”, Nature, Vol. 426, 2003, pp55.

[14]. N. Hur, S. Park, “Electric polarization reversal and memory in a multiferroic material induced by magnetic fields” Nature, Vol. 429,2004, pp392.

[15]. T. Arima , “Ferroelectricity Induced by Proper-Screw Type Magnetic Order”, Journal

[16]. Y. J. Choi, H. T. Yi, S. Lee, Q. Huang, V. Kiryukhin, Physical Review Letter, Vol.100, 2008,047601.

[17]. Nicola A. Spaldin, Sang-Wook Cheong, Ramamoorthy Ramesh „Multiferroics: past, present and future“ Physics Today, Vol. 63, 2010, pp38-43.

[18]. Fengzhen Huang, ZhijunWang, XiaomeiLu, JuntingZhang, KangliMin,WeiweiLin, Ruixia Ti, TingTingXu, Ju He, Chen Yue, Jinsong Zhu, “Peculiar magnetism of BiFeO3 nanoparticles with size approaching the period of the spiral spin structure”, Scientific Reports, Vol. 3, 2013, pp 2907.

[19]. Smolensky G A, Isupov V A, Agronovskaya A I, “A new group of ferroelectrics-(with layered structure)”, Journal of SovPhys Solid State, Vol. 1, 1959, pp149–150.

[20]. PPCurie, “Sur la symétrie dans les phénomènes physiques, symétrie d'un champ électrique et d'un champ magnétique”. Vol.3, 1894, pp393-415.

[21]. J. Valasek, “Piezo-electric and allied phenomena in Rochelle salt. Physical review”, Vol. 17, 1921, pp475.

[22]. T. O'dell, “The electrodynamics of magneto-electric media. Philosophical Magazine”, Vol. 7, 1962, pp1653-1669.79

[23]. I. Dzyaloshinskii, “Topological model of a heisenberg spin glass”, JETP Letters, Vol. 37, 1959, pp881-882.

[24]. D. Astrov, “The magnetoelectric effect in antiferromagnetics”, Sov. Phys. JETP, Vol. 11, 1960, pp708-709.

[25]. E. Ascher, H. Rieder, H. Schmid, and H. Stössel, “Some Properties of Ferromagnetoelectric Nickel-Iodine Boracite”, Journal of Applied Physics, Vol. 37, 1966, pp1404-1405.

[26]. G. Catalan and J.F. Scott, “Physics and applications of bismuth ferrite”, Advanced Materials, Vol. 21, 2009, pp2463-2485.

[27]. F. Kubel and H. Schmid, “Structure of a ferroelectric and ferroelastic monodomain crystal of the perovskite BiFeO3”, Acta crystallographica section B, Vol. 46, 1990, pp698-702.

[28]. A. Palewicz, I. Sosnowska, R. Przenioslo, and A. Hewat, “BiFeO3 crystal structure at low temperatures.”, Acta Physica Polonica-Series A General Physics, Vol. 117, 2010, p.296.

[29]. R.t. Shannon, “Revised effective ionic radii and systematic studies of interatomic distances in halides and chalcogenides”, Vol. 32, 1976, pp751-767.

[30]. F. Zavaliche, R. Das, D. Kim, C. Eom, S. Yang, PPShafer, and R. Ramesh, “Ferroelectric domain structure in epitaxial Bi Fe O 3 films” Applied Physics Letters, Vol. 87, 2005, pp182912.

[31]. J.R. Teague, R. Gerson, and W.J. James, “Dielectric hysteresis in single crystal BiFeO3. Solid zState Communications”, Vol. 8, 1970, pp1073-1074.

[32]. P.W. Anderson, “New approach to the theory of superexchange interactions”. Physical Review, Vol. 115, 1959, pp2.80

[33]. I.A. Sergienko and E. Dagotto, “Role of the Dzyaloshinskii-Moriya interaction in multiferroic perovskites”, Physical Review B, Vol. 73, 2006, pp094434.

[34]. D. Lebeugle, D. Colson, A. Forget, M. Viret, A. Bataille, and A. Gukasov, “Electricfield-induced spin flop in BiFeO 3 single crystals at room temperature”, Physical review letters, Vol.100, 2008, pp227602.

[35]. PPFischer, M. Polomska, I. Sosnowska, and M. Szymanski, “Temperature dependence of the crystal and magnetic structures of BiFeO3”, Journal of Physics C: Solid State Physics, Vol. 13, 1980, pp1931.

[36]. I. Sosnowska, T.PPNeumaier, and E. Steichele, “Spiral magnetic ordering in bismuth ferrite”, Journal of Physics C: Solid State Physics, Vol.15, 1982, pp4835.

[37]. S.M. Young, F. Zheng, and A.M. Rappe, “First-principles calculation of the bulk photovoltaic effect in bismuth

[38]. ferrite”, Physical review letters, Vol.109, 2012, pp236601.

[39]. W. Ji, K. Yao, and Y.C. Liang, “Evidence of bulk photovoltaic effect and large tensor coefficient in ferroelectric BiFeO 3 thin films”, Physical Review B, Vol. 84,2011, p.094115.

[40]. M. Qin, K. Yao, and Y.C. Liang, “Photovoltaic characteristics in polycrystalline and epitaxial (Pb 0.97 La 0.03) (Zr 0.52 Ti 0.48) O 3 ferroelectric thin films sandwiched

between different top and bottom electrodes", Journal of applied physics, 2009. Vol. 105, pp061624.

[41]. S. Yang, et al., Above-bandgap voltages from ferroelectric photovoltaic devices. Nature nanotechnology, Vol. 5,2010, pp143.

[42]. J. Wang, N. A. Spaldin, R. Ramesh, "Epitaxial BiFeO3 Multiferroic Thin Film Heterostructures" J. Science, Vol. 299, 2003, pp1719.

[43]. [30]. J. Lu, L. J. Qiao, PPZ. Fu, Y. C. Wu, "Phase equilibrium of Bi2O3–Fe2O3 pseudo-binary system and growth of BiFeO3 single crystal", Journal of Crystal Growth Vol. 318, 2011, pp936-941

[44]. [72]. M. Ichiki, Y. Morikawa, Y. Mabune, and T. Nakada, Electrical properties of photovoltaic lead lanthanum zirconate titanate in an electrostatic-optical motor application, Journal of the European Ceramic Society, Vol. 24, 2004, p1709-1714.

[45]. [69]. S. Gupta, M. Tomar, and V. Gupta, Ferroelectric photovoltaic properties of Ce and Mn cooped BiFeO3 thin film. Journal of Applied Physics, 2014. Vol. 115(1), pp014102.

[46]. [70]. V.M. Fridkin, Photoferroelectrics. Vol. 9. 2012: Springer Science & Business Media.

[47]. [71]. P.S. Brody, Semiconductor-ferroelectric nonvolatile memory using anomalous high photo voltages in ferroelectric ceramics. Applied Physics Letters, Vol. 38, 1981, p153-155.

[48]. D.I.Khomskii, "Magnetism and ferroelectricity: why do they so seldom coexist?" Bulletin of American Physical Society C, Vol. 1, 2001, pp. 21002.

[49]. José Luis Ortiz-Quiñonez, David Díaz, Inti Zumeta-Dubé, Humberto Arriola-Santamaría, Israel Betancourt, Patricia Santiago-Jacinto, Noel Nava-Etzana „Easy synthesis of high- purity BiFeO3 nanoparticles: new insights derived from the structural, optical, and magnetic characterization" Inorganic Chemistry, Vol. 52, 2013, pp10306-10317.